

THE USE OF GOLD AND SILVER NANOPARTICLES FOR
SURFACE ENHANCED FLUORESCENCE (SEF) OF DYES

A THESIS SUBMITTED TO
THE GRADUATE SCHOOL OF NATURAL AND APPLIED SCIENCES
OF
MIDDLE EAST TECHNICAL UNIVERSITY

BY

TACETTİN ÖZTÜRK

IN PARTIAL FULFILLMENT OF THE REQUIREMENTS
FOR
THE DEGREE OF MASTER OF SCIENCE
IN
THE DEPARTMENT OF CHEMISTRY

SEPTEMBER 2010

Approval of the thesis:

**THE USE OF GOLD AND SILVER NANOPARTICLES FOR SURFACE
ENHANCED FLUORESCENCE (SEF) OF DYES**

submitted by **TACETTİN ÖZTÜRK** in partial fulfillment of the requirements for
the degree of **Master of Science in Chemistry Department, Middle East
Technical University** by,

Prof. Dr. Canan Özgen
Dean, Graduate School of **Natural and Applied Sciences** _____

Prof. Dr. İlker Özkan
Head of Department, **Chemistry** _____

Prof. Dr. Mürvet Volkan
Supervisor, **Chemistry Department, METU** _____

Examining Committee Members:

Prof. Dr. Erdal Bayramlı
Chemistry Department, METU _____

Prof. Dr. Mürvet Volkan
Chemistry Department, METU _____

Prof. Dr. Mehmet Parlak
Physics Department, METU _____

Prof. Dr. Ceyhan Kayran
Chemistry Department, METU _____

Prof. Dr. Necati Özkan.
Central Laboratory, METU _____

Date: September 06, 2010

I hereby declare that all information in this document has been obtained and presented in accordance with academic rules and ethical conduct. I also declare that, as required by these rules and conduct, I have fully cited and referenced all material and results that are not original to this work.

Name, Last Name: Tacettin Öztürk

Signature:

ABSTRACT

THE USE OF GOLD AND SILVER NANOPARTICLES FOR SURFACE ENHANCED FLUORESCENCE (SEF) OF DYES

Öztürk, Tacettin

M.Sc., Department of Chemistry

Supervisor: Prof. Dr. Mürvet Volkan

September 2010, 81 pages

This study focuses on preparing surface enhanced fluorescence (SEF) substrates for use in the enhancement of the emission signal of rhodamine B and fluorescein dyes.

Fluorescence spectroscopy has been widely utilized owing to its high sensitivity. SEF is a process where the interactions of fluorophores with the localized surface plasmons of metal nanoparticles results in fluorescence enhancement, increased photostability and rates of system radiative decay which leads to a decreased lifetime. One of the most important factors of SEF studies is to provide a uniform distance between fluorophore and metal nanoparticle in a controlled manner; otherwise, Förster resonance energy transfer takes place from fluorophore to metal nanoparticle and emission intensity of fluorophore is quenched.

The spherical gold and silver nanoparticles were prepared using the well known and straightforward chemical reduction method, in which sodium citrate acted both as a reducing agent and a stabilizer around the formed nanoparticles. Silver and gold were chosen because of their high plasmon field enhancement. Since plasmon field strongly depends on the shape and size of the nanoparticles, the prepared

nanoparticles were characterized using absorption spectroscopy and field emission scanning electron microscopy (FE-SEM).

Prior to deposition of silver or gold nanoparticles on glass slides, the slides were derivatized by immersing them into an aqueous solution of 3-Aminopropylethoxysilane (APTES). Following derivatization, silver or gold nanoparticles were deposited by immersing the slides into the colloid mixture. Metal nanoparticle coated slides were characterized using absorption spectroscopy and field emission scanning electron microscopy (FE-SEM). Surface enhanced Raman scattering (SERS) measurements were carried out to observe the plasmon efficiency of the deposited nanoparticles. The SERS measurements were repeated for the duration of two weeks in order to check the stability of the plasmon efficiency.

In this study, different types of materials (silica, zinc oxide, gold, stearic acid.) were employed as spacers to observe their effects on fluorescence enhancement. Physical vapor deposition (PVD) and Langmuir-Blodgett (LB) film deposition techniques were used for the formation of the spacer within the substrate.

Fluorescence enhancement of rhodamine B and fluorescein was observed on the prepared SEF substrates. Obtained enhancement factors indicate that SEF substrates have the potential for sensitivity improvements of fluorescence sensing in many fields.

Keywords: Silver, gold, nanoparticles, plasmon, surface enhanced fluorescence (SEF) substrate, Förster resonance energy transfer (FRET), spacer, PVD, Langmuir-Blodgett, rhodamine B, fluorescein

ÖZ

ALTIN VE GÜMÜŞ NANOPARÇACIKLARIN BOYALARDA YÜZEYDE GÜÇLENDİRİLMİŞ FLORESANS ÇALIŞMALARI İÇİN KULLANIMI

Öztürk, Tacettin

Yüksek Lisans, Kimya Bölümü

Tez Yöneticisi: Prof. Dr. Mürvet Volkan

Eylül 2010, 81pages

Bu çalışmanın odak noktası, rodamin B ve fluoresin boyaalarının emiyon sinyallerinin güçlendirilmesi için, yüzeyde güçlendirilmiş floresans (YGF) substratların hazırlanmasıdır.

Fluoresans spektroskopisi sahip olduđu duyarlılığı sayesinde geniş bir alanda kullanılmaktadır. YGF, floroforların metal nanoparçacıkların yerleşik yüzey plasmonları ile karşılıklı etkileşimi sonucu floresans şiddetinin güçlendirilmesi, fotokararlılığın ve ışıklı salınım hızının artmasına bağlı olarak yaşam süresinin azalması gibi sonuçlara sebep olan bir olgudur. YGF araştırmalarında en önemli faktörlerden biri, florofor ile metal nanoparçacık arasında düzgün ve homojen bir uzaklığın oluşturulmasıdır. Aksi takdirde florofordan metal nanoparçacığa Förster rezonans enerji transferi gerçekleşir ve floroforun ışımaya sinyali söndürülür.

Küresel altın ve gümüş nanoparçacıklar kolay ve iyi bilinen kimyasal indirgeme metodu kullanarak hazırlanmıştır. Kullanılan bu metotta, sodyum sitrat hem indirgeyici hem de oluşan nanoparçacıkların daha kararlı hale getirilmesinde etken ajan olarak görev almıştır. Gümüş ve altın nanoparçacıklar sahip oldukları yüksek plasmon alan güçlendirmesi nedeniyle seçilmiştir. Plasmon alanı nanoparçacığın

şekli ve boyutuna bağlı olduğu için, hazırlanan nanoparçacıklar optik absorpsiyon spektroskopisi ve alan emisyonlu taramalı elektron mikroskobu (AE-TEM) kullanarak karakterize edilmiştir.

Gümüş ve altın nanoparçacıkların cam slayt yüzeyine kaplanmasından önce, cam slaytlar 3-aminopropiltrietoksisilan sulu çözeltisi içine daldırılarak modifiye edilmiştir. Modifiye işleminin ardından cam slaytlarının yüzeyinin gümüş ve altın nanoparçacıklarla kaplanması, slaytların kolloid karışımlara daldırılmasıyla yapılmıştır. Gümüş veya altın nanoparçacık kaplı cam slaytlar, optik absorpsiyon spektroskopisi ve alan emisyonlu taramalı electron mikroskobu (AE-TEM) kullanarak karakterize edilmiştir. Yüzeyde güçlendirilmiş Raman saçılımı (YGRS) ölçümleri, yüzeyde tutturulmuş metal nanoparçacıkların plasmon verimliliğinin gözlemlenmesi için uygulanmıştır. Ayrıca, plasmon verimliliğinin kararlılığını kontrol etmek için YGRS ölçümleri tekrarlanmıştır.

Bu çalışmada, floresans güçlendirmesine etkilerini incelemek için farklı malzemelerden (silika, çinko oksit, altın, stearik asit) ara katmanlar (spacer) kullanılmıştır. Fiziksel buhar biriktirme (FBB) ve Langmuir-Blodgett tek katman kaplama teknikleri substrat üstünde ara katmanın oluşturulması için kullanılmıştır.

Rodamin B ve floresin maddelerinin güçlendirilmiş floresansı, hazırlanan YGF substratlar üstünde gözlemlenmiştir. Elde edilen güçlendirme faktörleri, hazırlanan YGF substratların birçok alandaki floresans algılamalarının duyarlılığını iyileştirmede potansiyeli olduğunu göstermiştir.

Anahtar Kelimeler: Gümüş, altın, nanoparçacık, plasmon, yüzeyde güçlendirilmiş floresans (YGF), substrat, Förster rezonans enerji transferi, FBB, Langmuir-Blodgett, rodamin B, floresin

To Bülent Atamer

ACKNOWLEDGEMENTS

I wish to express my sincere gratitude to my advisor Professor Dr. Mürvet Volkan for her excellent guidance, valuable advice, limitless encouragement, during the course of M.Sc. study. Working with her has been an enjoyable, unique and valuable learning experience which I will treasure throughout my life.

I would deeply like to thank Prof. Dr. Mehmet Parlak and Mustafa Kulakçı for their invaluable contributions, suggestions and understandings.

I would like to thank my lab mates; Murat Kaya, Seher Karabıçak, Seda Kibar, Sezen Keser, Ümit Zengin, Mervegül Maden, Üzeyir Doğan, Zehra Tatlıcı and all C-50 research group members for their contributions and friendship. Thanks to them I never felt alone during this study. Also I thank to Emrah Yıldırım and all AtaMAN research group members for their help and friendship.

I would like to thank my friend Ufuk Özgen. I always feel happy to have met him in physics course in freshman year and became a friend.

I would deeply like to thank my flatmates; Mustafa Emre Boysan and Özgür Cem Ceylan, Hüseyin Emrah Taşlı for their friendship.

Also great thanks to my colleague Onur İşcan and Çağrı İlçe, it is always a pleasure to talk with them.

Huge thanks to my family for the limitless freedom they provide.

And special thanks to A. Gizem Erbuğa.

TABLE OF CONTENTS

ABSTRACT.....	IV
ÖZ	VI
ACKNOWLEDGEMENTS	IX
TABLE OF CONTENTS	X
LIST OF TABLES	XIII
LIST OF FIGURES	XIV
CHAPTERS	1
1. INTRODUCTION.....	1
1.1 Micro and Nanotechnology	1
1.1.1 Applications of Nanotechnology	3
1.2 Nanomaterials	3
1.3 The Surface Plasmon	5
1.4 Surface Plasmon Enhanced Spectroscopy	6
1.4.1 Surface Enhanced Raman Scattering (SERS) Spectroscopy	7
1.4.2 Surface Enhanced Fluorescence.....	9
1.4.2.1 History of Fluorescence	9
1.4.2.2 History of Enhanced Fluorescence	10
1.4.2.3 Principles of Surface Enhanced Fluorescence (SEF)	10
1.4.2.4 Applications of Surface Enhanced Fluorescence (SEF).....	17
1.4.2.5 Recent Studies on SEF and Enhancement Factors (EF) achieved	17
1.5 Thin Film Deposition Techniques	20
1.5.1 Physical Vapor Deposition (PVD).....	20
1.5.2 Langmuir-Blodgett (LB) Film Formation.....	21
1.6 Aim of the Study.....	22

2. EXPERIMENTAL	23
2.1 Chemical and Reagents.....	23
2.2 Instrumentation	24
2.2.1 Fluorescence Spectrometer	24
2.2.2 UV-VIS Spectrometer.....	25
2.2.3 Centrifuge.....	25
2.2.4 Surface Enhanced Raman Spectrometer (SERS).....	26
2.2.5 Field Emission Scanning Electron Microscopy (FE-SEM)	26
2.2.6 Physical Vapor Deposition System (by Sputtering Method)	27
2.2.7 Physical Vapor Deposition System (by Evaporation Method)	27
2.2.8 Langmuir-Blodgett Film Formation System.....	27
2.3 Preparation of Nanoparticles	28
2.3.1 Silver Colloid	28
2.3.2 Gold Colloid.....	28
2.3.3 Silica Coated Silver Colloid.....	29
2.4 Preparation of Fluorescence Solutions	29
2.5 Preparation of Glass Slides	29
2.5.1 Cleaning of Slides	29
2.5.2 Etching the Slides.....	29
2.5.3 Derivatization (Modification) of the Slides	30
2.6 Deposition of Metal Nanoparticles onto Derivatized (Modified) Slides.....	31
2.7 Deposition of Spacer (Distance Layer) onto Metal Nanoparticle Coated Slides.....	31
2.7.1 Physical Vapor Deposition of Silica and Zinc oxide Layers by Sputtering	32
2.7.2 Physical Vapor Deposition of Gold by Thermal Evaporation	32
2.7.3 Formation of Stearic Acid Molecular Layers by Langmuir-Blodgett Film System	33
2.7.3.1 Cleaning and Preparation of Langmuir-Blodgett Film System.....	33
2.7.3.2 Isotherm Measurements.....	34
2.7.3.3 Dipping (Coating) Experiments	35
2.8 Surface Enhanced Raman Scattering (SERS) Measurements	36

3. RESULTS AND DISCUSSION	37
3.1 Properties of Metal Nanoparticles	38
3.1.1 Silver Nanoparticles	38
3.1.2 Gold Nanoparticles.....	42
3.1.3 Silica Coated Silver Nanoparticles	44
3.2 Etching Process.....	45
3.3 Derivatization (Modification) of the Glass Slides	46
3.4 Deposition of Nanoparticles on Modified Slides.....	47
3.4.1 Immersion Time Optimization – FE-SEM.....	47
3.4.2 Absorption Spectra of Metal Nanoparticle Coated Slides	50
3.5 Use of Metal Nanoparticle Coated Surface as a Surface Enhanced Raman Scattering (SERS) Substrate	51
3.5.1 Immersion Time Optimization - SERS	52
3.5.2 Stability of Silver Nanoparticle Coated Substrates	54
3.6 Preparation and Evaluation of Surface Enhanced Fluorescence (SEF) Substrates	55
3.6.1 Silica and Zinc oxide Layers on Silver Nanoparticle Coated Substrates	55
3.6.2 Gold Layer on Silver Nanoparticle Coated Substrates	57
3.6.3 Formation of Stearic Acid Molecular Layers on Silver Nanoparticles Coated Substrates	57
3.6.3.1 Isotherm Experiments and Target Surface Pressure.....	58
3.6.3.2 Dipping Experiments.....	59
3.7 Surface Enhanced Fluorescence (SEF) Studies	62
3.7.1. Fluorescence Properties of Rhodamine B and Fluorescein	62
3.7.2 SEF in Solution	64
3.7.3 SEF on Surface.....	68
3.7.3.1 Distance Optimization	69
3.7.3.2 Evaluation of Different Materials as a Spacer.....	71
4. CONCLUSION	74
5. REFERENCES.....	76

LIST OF TABLES

TABLES

Table 1.1 List of recent surface enhanced fluorescence studies.....	18
Table 3.1 The components of prepared SEF substrates	37
Table 3.2 Maximum absorption wavelength (λ_{max}) and amount of 1 % (w/v) of $Na_3C_6H_5O_7$ aqueous solution (V).....	41
Table 3.3 TR values obtained after 5 layers of stearic acid deposited.	61
Table 3.4 Silica thickness and obtained enhancement factors	70
Table 3.5 Enhancement Factors with varying number stearic acid layers in SEF substrates	73

LIST OF FIGURES

FIGURES

Figure 1.1 Image of the first digital computer, ENIAC [3].....	1
Figure 1.2 The Lycurgus Cup, when light reflected (a) and transmitted (b) [12].....	4
Figure 1.3 Schematic representation of plasmon oscillation of a spherical metal nanoparticle	5
Figure 1.4 Transmission Electron Microscopy (TEM) micrographs of gold nanospheres (a), nanorods (b) and nanoprisms (c), images of AuAg alloys with increasing gold ratio (d), gold nanorods with increasing aspect ratio (e), Ag nanoprism with increasing lateral size (f) [17]	6
Figure 1.5 Schematic representation of surface enhanced Raman scattering (SERS)	8
Figure 1.6 The fluorometer to determine the quinine amount during World War II .	9
Figure 1.7 Schematic representations of fluorescence and surface enhanced fluorescence.....	11
Figure 1.8 Jablonski diagram (a) fluorophore alone, (b) fluorophore located near metal nanoparticle	14
Figure 1.9 Plasmon absorption of spherical gold nanoparticles with different sizes [36].....	15
Figure 1.10 The effect of distance to enhancement	15
Figure 2.1 Sample geometry of fluorescence measurements for (a) solution (b) surface enhanced fluorescence	24
Figure 2.2 Homemade stand for incident light angle optimization, (a) top, (b) front view	25
Figure 2.3 Raman spectroscopy [67].....	26
Figure 2.4 Sputtering system [68]	27
Figure 2.5 Langmuir-Blodgett film formation system [69]	28
Figure 2.6 Schematic representation of (a) not etched and (b) etched surface	30
Figure 2.7 Schematic representation of surface derivatization	30
Figure 2.8 Deposition of metal nanoparticles on modified slide by immersion method.....	31

Figure 2.9 Sputtering system (Inside the chamber).....	32
Figure 2.10: Thermal evaporation system.....	33
Figure 2.11 Isotherm experiment (Compression of Langmuir Monolayer), (a) stearic acid monolayer in “gaseous phase” (b) stearic acid monolayer in “solid phase”	34
Figure 2.12 Dipping experiment	36
Figure 3.1 Image of silver colloid	38
Figure 3.2 Absorption spectrum of silver colloid	39
Figure 3.3 Absorption spectra of silver colloids, addition of different amount of 1% (w/v) of $\text{Na}_3\text{C}_6\text{H}_5\text{O}_7$ aqueous solution	40
Figure 3.4 FE-SEM image of silver nanoparticles deposited on glass slide	41
Figure 3.5 Image of gold colloid.....	42
Figure 3.6 Absorption spectrum of gold colloid	42
Figure 3.7: FE-SEM image of gold nanoparticles deposited on glass slide.....	43
Figure 3.8 FE-SEM image of silica coated silver nanoparticles deposited on glass slide	44
Figure 3.9 FE-SEM images of silver nanoparticles on etched and not-etched glass slides.....	45
Figure 3.10 Deposition of silver nanoparticles on (a) unmodified and (b) modified surface	46
Figure 3.11 Absorption spectra of silver nanoparticles on modified and unmodified surface	47
Figure 3.12 FE-SEM images of gold nanoparticles deposited on slides, (a) 1 hour (b) 3 hours (c) 6 hours (d) 12 hours (e) 18 hours (f) 24 hours immersion time.....	48
Figure 3.13 FE-SEM images of silver nanoparticles deposited on slides, (a) 1 hour (b) 3 hours (c) 6 hours (d) 12 hours (e) 18 hours (f) 24 hours immersion time.....	49
Figure 3.14 Absorption spectrum of silver nanoparticles coated glass slide (18 hours of immersion).....	50
Figure 3.15 Absorption spectrum of gold nanoparticles coated glass slide (9 hours of immersion).....	51
Figure 3.16 Effect of silver nanoparticles coated surface on SERS intensities of 1.0×10^{-6} M Brilliant Cresyl Blue (BCB) drop, (a) on glass, (b) on silver nanoparticles (NP) coated glass surface	52

Figure 3.17 Effect of nanoparticle deposition immersion time on the SERS signal enhancing of silver nanoparticles coated substrates on BCB.....	53
Figure 3.18 SERS intensity of 10^{-6} M BCB solution versus immersion time (h) graph.....	53
Figure 3.19 Raman spectra of BCB on freshly prepared silver nanoparticle coated substrate and two weeks later.....	54
Figure 3.20 Absorption spectra of silver nanoparticles coated substrates with different thickness of silica layers.....	55
Figure 3.21 Absorption spectra of (a) silver nanoparticles coated substrate (b) 10 nm ZnO coated on silver nanoparticles coated substrate.....	56
Figure 3.22 Absorption spectra of (a) 10 nm gold deposited silver nanoparticles coated substrates, (b) only silver nanoparticles coated substrate, (c) only 10 nm gold deposited substrate.....	57
Figure 3.23 Surface pressure – Mean molecular area per stearic acid molecule (π -A) isotherm of stearic acid monolayer (green line), region (a) solid , (b) liquid (c) gas phase.....	58
Figure 3.24 Y-type LB deposition of stearic acid layers, (a) 1 layer, (b) 2 layers, (c) 3 layers, (d) 4 layers (e) 5 layers.....	59
Figure 3.25 Graph of transfer ratio, barrier, position versus layer no.....	60
Figure 3.26 Position of barriers (a) zero position, (b) at target surface pressure, (c) at the end of dipping experiment.....	61
Figure 3.27 Excitation and emission spectra of rhodamine B.....	62
Figure 3.28 Excitation and emission spectra of fluorescein.....	63
Figure 3.29 Effect of silver colloid to the fluorescence of 10^{-7} M fluorescein solution.....	64
Figure 3.30 Effect of gold colloid to the fluorescence of 10^{-7} M fluorescein solution.....	64
Figure 3.31 Effect of silver colloid to the fluorescence of 10^{-6} M rhodamine B solution.....	65
Figure 3.32 Effect of gold colloid to the fluorescence of 10^{-6} M rhodamine B solution.....	66

Figure 3.33 Effect of silica coated silver colloid to the fluorescence of 10^{-6} M rhodamine B solution	67
Figure 3.34 Incident light angle optimization for SEF measurements.....	68
Figure 3.35 Distance optimization by silica layer between silver nanoparticles and rhodamine B molecules.....	69
Figure 3.36 Enhanced fluorescence of fluorescein	70
Figure 3.37 Effect of different spacer materials (10 nm thickness) to the fluorescence signal of rhodamine B.....	71
Figure 3.38 Effect of number of stearic acid (SA) layers the enhanced fluorescence of 5×10^{-5} M Rhodamine B solution	72

CHAPTER 1

INTRODUCTION

1.1 Micro and Nanotechnology

During the last 50 years of scientific progress, countless inventions in the form of devices, equipment, tools and various other technological systems have been conceived, realized and produced. As the need for mobility and practical sizes emerged, these new objects started to get smaller, following the pace of development in miniaturization technologies and micro and nanotechnology [1].

The first digital computer, ENIAC (Electronic Numerical Integrator and Computer) was designed and built by J. Presper Eckert and John Mauchly at the University of Pennsylvania in 1946. ENIAC (Figure 1.1) was 50 tons [2]. Today, a notebook PC – needless to say, infinitely more capable than ENIAC- weighing 2.5 kg is considered to be heavy for practical purposes.



Figure 1.1 Image of the first digital computer, ENIAC [3].

Microtechnology has had impacts in many other areas. For instance, sub-micron size range is made visible to the human eye by using optical microscopes. However, the resolution provided by these devices is not sufficient alone for today's requirements. Instruments that provide single atom or single molecule detection were developed by means of microtechnology [4].

Nanoscience is an interdisciplinary research area which focuses on matter at the molecular or atomic level. The distinctive properties encountered at nanoscale caught the attention of scientists. These properties of matter display a potential of new applications, innovations and inventions in the future. Due to this huge potential, nanoscience is getting more and more popular each day.

The term nanotechnology was first used by the physicist Richard Feynman in 1959. In one of his talks he introduced a molecular machine built with atomic precision. In 1974, Norio Tanuguchi used *nanotechnology*, in his articles about ion-sputter machining. Nanotechnology is the production, characterization, application of systems, structures and devices by controlling structure and size at the nanoscale. It is reported that the majority of studies in this field deal with nanomaterials with sizes ranging from 1 to 100 nm, because it is this size range within the nanoscale that, nanomaterials has the greatest potential to show their special properties that differentiate them. [5]

The Scanning Tunneling Microscope (STM) and the Atomic Force Microscope (AFM) which enabled researchers to examine and view matter at the nanoscale, were introduced in 1981 and 1986, respectively. These inventions prompted a major increase in the amount of research done on nanotechnology. [6]

Today, it may be said that nanotechnology stands in a place of its own within the natural sciences. A definitive nanotechnology research project asks for the cooperation of researchers working in many different fields of science. In other words, nanotechnology is the meeting point of different branches of sciences where the boundaries are not clear [7].

1.1.1 Applications of Nanotechnology

Drug delivery, tissue engineering and diagnostic techniques are among some of the areas in medicine which nanotechnology has become an integral part of. Magnetic nanoparticles (iron, iron oxide, cobalt, etc.) have been used for the treatment of cancer in medicine. Carbon nanotubes with their strength are used in automotive and aerospace industry and due to their electrical properties; they are used in flat screen displays and sensing devices. Nanoparticles (lanthanum, cerium, silicon, etc.) are also used in fuel cells and solar energy cells [8]. Catalysis and filtration are other fields where nanotechnology has a significant role.

Along many other global challenges, global climate change and its proposed consequences in the near future impose a huge responsibility on researchers today. With the contribution of nanotechnology, the development of solar cells, semiconductors, fuel cells and various other innovations have a great chance of increasing the efficiency of energy production, leading in the establishment of environmentally friendly systems [9].

1.2 Nanomaterials

A general definition of nanostructure can be given as a structure with one dimension below 100 nm and another dimension below 1 μm [4].

Nanomaterials can be classified as zero-dimensional (nanoparticles), one dimensional (nanotubes and nanorods) and two dimensional (thin films) [10].

Although the term nanotechnology was coined in 1959, the first manmade nanomaterial was used in fourth century by Romans without an understanding of the physics behind it. Lycurgus Cup (Figure 1.2) is made of dichroic glass. The cup has green color when light is reflected from it but it turns red when light is made to pass through it instead. For many years, it has been thought that the cup was not made of glass due to its dichroic property. In 1981, a sample was taken from the cup and analyzed. Results showed that the glass that the cup was made from contains silver and gold nanoparticles with 50-100 nm size [11].

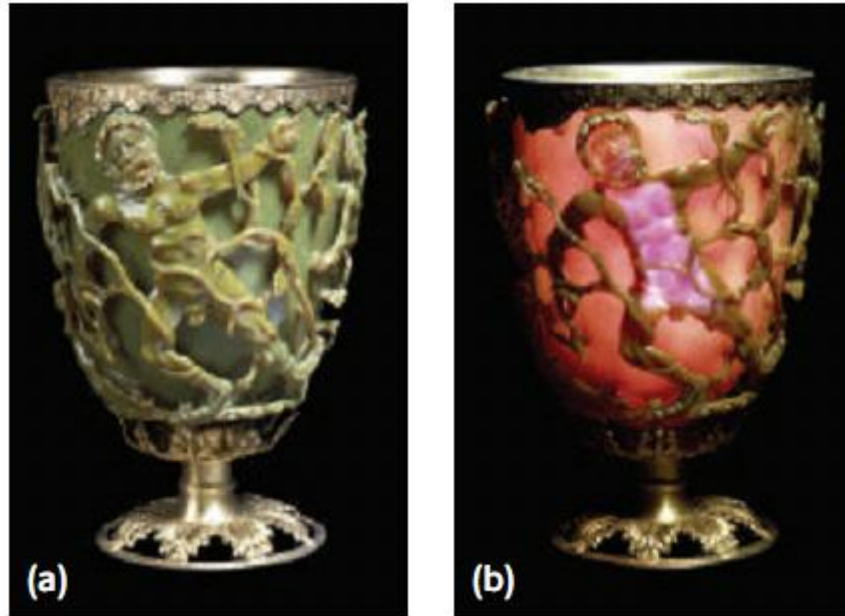


Figure 1.2 The Lycurgus Cup, when light reflected (a) and transmitted (b) [12].

Nanomaterials have gained huge attention due to their properties that differentiate them from bulk materials. The properties of nanomaterials are size-dependent. As size decreases, the ratio of the number of atoms on the surface to the number of atoms in the bulk increases. This increase in the amount of surface atoms will provide higher surface energy.

When the mechanical properties are compared, metal nanomaterials are stronger than bulk metals. It has also been shown that electronic, optical and magnetic properties of nanostructures are different than bulk materials.

1.3 The Surface Plasmon

Surface plasmons (SPs) are electromagnetic surface waves propagating between interfaces of metal and a dielectric material by the motions of electrons (Figure 1.3) [13]. The resonance frequency of a plasmon, which depends on the morphology of the metal nanoparticle, can be tuned by changing the shape and size of metal nanoparticles [14].

When the properties of material and boundary conditions are given correctly, the surface plasmon can be defined by using the Maxwell equations [15]. The solution of Maxwell's equations to the extinction spectra of spherical metal nanoparticles with known size is proposed by Hergertt Mie in 1908 [16].

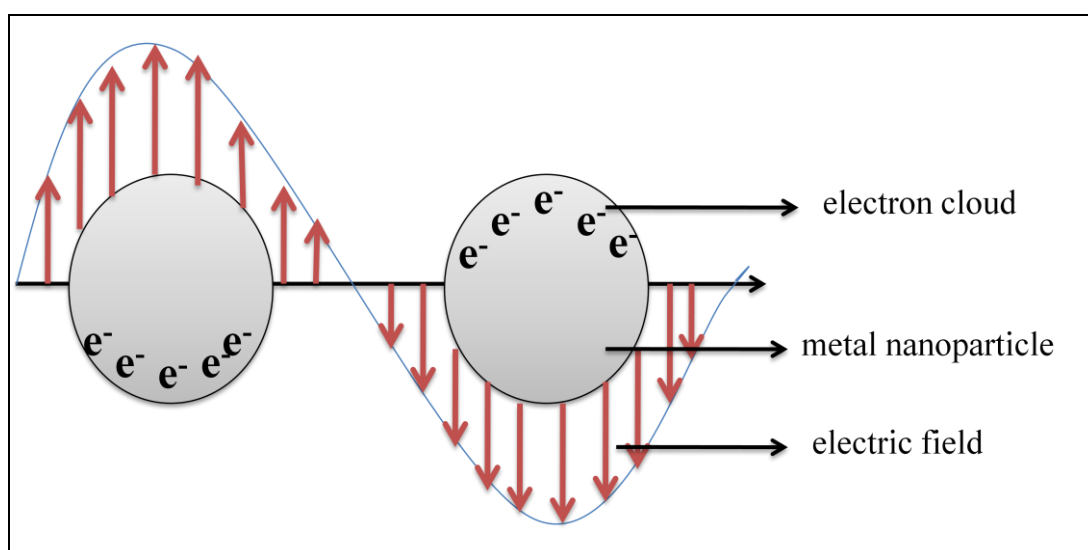


Figure 1.3 Schematic representation of plasmon oscillation of a spherical metal nanoparticle [13].

The color of metal nanoparticles changes when their sizes are changed (Figure 1.3). Gold, silver, copper and some alkali metal nanoparticles have absorption maximum in the visible range. Deformation from spherical shape will result in another plasmon band. For example, nanorods have two plasmon bands due to the longitudinal and transverse electron oscillations [17].

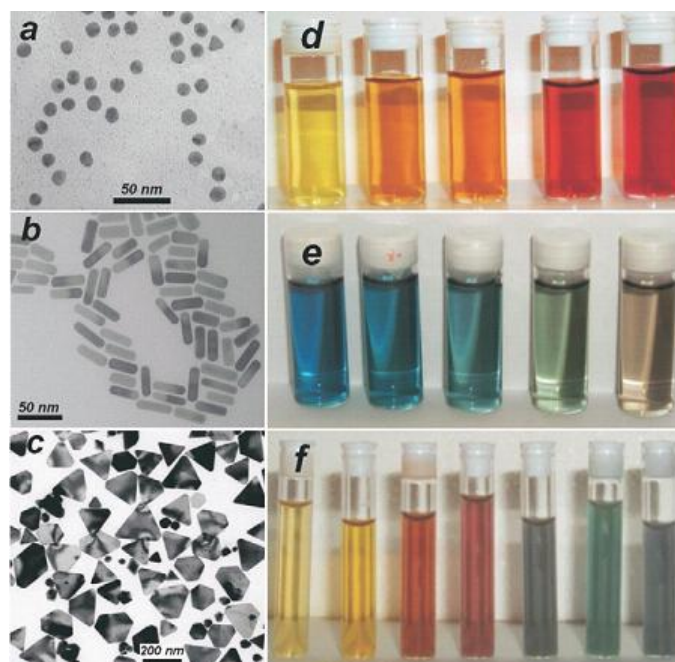


Figure 1.4 Transmission Electron Microscopy (TEM) micrographs of gold nanospheres (a), nanorods (b) and nanoprisms (c), images of AuAg alloys with increasing gold ratio (d), gold nanorods with increasing aspect ratio (e), Ag nanoprism with increasing lateral size (f) [17].

1.4 Surface Plasmon Enhanced Spectroscopy

The presence of plasmons around metal nanoparticles provides the enhancement of radiation. The electromagnetic field of plasmons on the nanoparticles account for different types of surface phenomena. These surface phenomena have been exploited in spectroscopic techniques for the last 25 years. The most well-known plasmon enhanced spectroscopic techniques are surface enhanced infrared absorption (SEIRA), surface enhanced Raman scattering (SERS) and surface enhanced fluorescence (SEF).

E_0 is given as the electric field of incident light, and the local electric field in presence of metal nanoparticles is $E_L = g E_0$, where g is the enhancement factor. Enhancement factor is defined as the magnitude of increase in radiation when the molecule is close to metal nanoparticles.

If the wavelength of incident light is in resonance with the surface plasmons of metal nanoparticles, then g will be higher than 1.0 [15]. g value has been estimated between 10^{-10} - $10^{2.5}$ [16].

1.4.1 Surface Enhanced Raman Scattering (SERS) Spectroscopy

Surface enhanced Raman scattering (SERS) (Figure 1.5) was discovered by Fleischmann et al. [18] in 1974. In his experiments, Fleischmann observed enhanced Raman scattering of pyridine on roughened silver surface. His initial idea on the results was that the signal intensity increased because the number of pyridine molecules adsorbed on the surface is higher due to the higher surface area of the roughened surface than a smooth one. He furthered his studies to prove that the observed enhancement was actually due to the presence of metal nanoparticles.

The order of the enhancement levels observed were relatively high in these initial experiments (10^6 - 10^{12}), and understanding the mechanism of SERS became an important issue from the beginning of the discovery. Explanations were proposed as electromagnetic enhancement by Jeanmaire and van Duyne [19], and chemical enhancement by Albert and Creighton [20].

In the chemical effect, it is stated that enhancement is due to charge transfer between chemisorbed molecule and adsorbent metal nanoparticles [21]. However, this approach is not applicable when there is no chemical bond between molecule and metal nanoparticles, even though enhancement may be observed under such conditions. Therefore, the electromagnetic effect approach is widely accepted for explaining SERS phenomena. In the electromagnetic effect approach, the surface plasmons are excited by incident light and field enhancement occurs

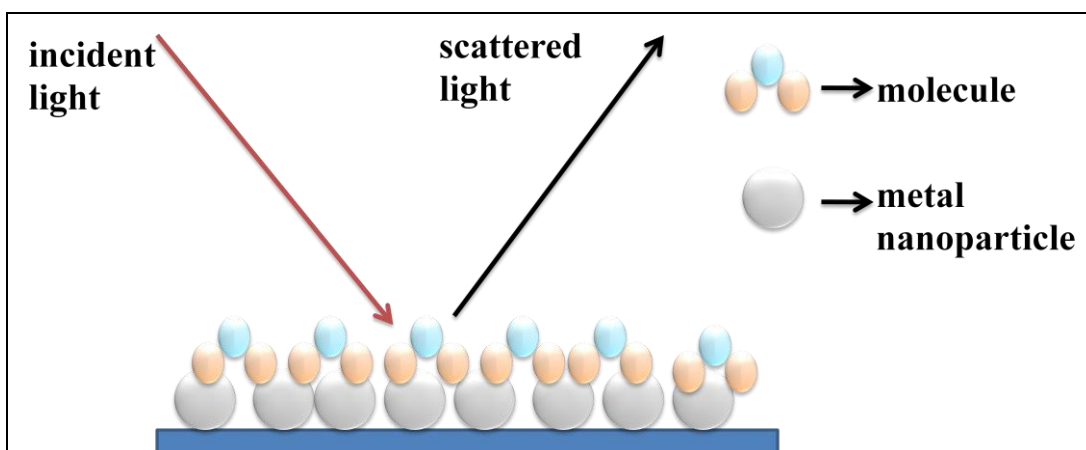


Figure 1.5 Schematic representation of surface enhanced Raman scattering (SERS)

In the first decade of its discovery, there was huge interest in SERS. Although the enhancement factor was confirmed to be very high, the amount of research decreased in the following years due to the irreproducibility encountered in early systems. Advances in nanofabrication (preparation of uniform substrates controlled in the nanoscale) along with improvements in detection technologies providing higher resolution and sensitivity presented researchers with the possibility to conduct experiments with precision. SERS studies became a research focus once again towards the end of 1990s and research has been increasing until today.

In most of the SERS studies gold, silver and copper metal nanoparticles are chosen as a plasmon source. Silver is preferred more often than gold and copper due to its high plasmon intensity.

1.4.2 Surface Enhanced Fluorescence

1.4.2.1 History of Fluorescence

Fluorescent materials have been in use for thousands of years without an understanding of the science surrounding it. Sir George Stokes was the first who applied a scientific approach to fluorescence in 1852. He found out that the emission wavelength was larger than the excitation wavelength. The first fluorimetric analysis was performed by F. Goppelsröder in 1867 to determine Al (III) by the fluorescence of its morin chelate.

In 1887 fluorescence was used to trace ground waters. 10 kg of fluorescein was introduced at a chosen point and 60 hours of later it appeared in another observation point. The first fluorescence microscope was developed by Otto Heimstaedt and Heinrich Lehmann in 1913.



Figure 1.6 The fluorometer to determine the quinine amount during World War II.

During World War II, in a United States government research program to find an alternative treatment for malaria scientists used a fluorometer (Figure 1.6) to determine the amount of quinine -which was the best known remedy at the time- in a patient's plasma [22].

1.4.2.2 History of Enhanced Fluorescence

The first observation of enhancement of fluorescence radiation by fluorophores in close proximity to metal nanoparticles was studied by Drexhage et al. [23]. The article showed when a fluorophore was placed at a distance to a silver film with nanosize thickness, the emission intensity of fluorophore increased depending on the distance between the metal film and fluorophore. However, the fluorescence enhancement was not impressive when compared with SERS enhancement factors. Consequently, while there was a lot of research focused on SERS, only little research effort was put into SEF.

On the other hand, advances in biotechnology in the course of the last 20 years, and an ongoing motivation in lowering analytical detection limits aid in fluorescence becoming one of the dominant detection methods.

In nomenclature, enhanced fluorescence due to plasmons of metal nanoparticles is named metal enhanced fluorescence (MEF) [24], resonance enhanced fluorescence (REF) [25] or surface enhanced fluorescence (SEF) [26]. In this thesis, SEF is preferred as it is in better conjunction with the term SERS.

1.4.2.3 Principles of Surface Enhanced Fluorescence (SEF)

Fluorescence is a two stage process. There is excitation by absorption of light and relaxation by emission of light. The interaction of fluorophore with metal nanoparticles effects both absorption and emission steps [27].

Surface enhanced fluorescence is a promising technique which utilizes the positive effect of metal nanoparticles on the fluorescence signal of fluorophore in order to increase the sensitivity of traditional fluorescence techniques (Figure 1.7).

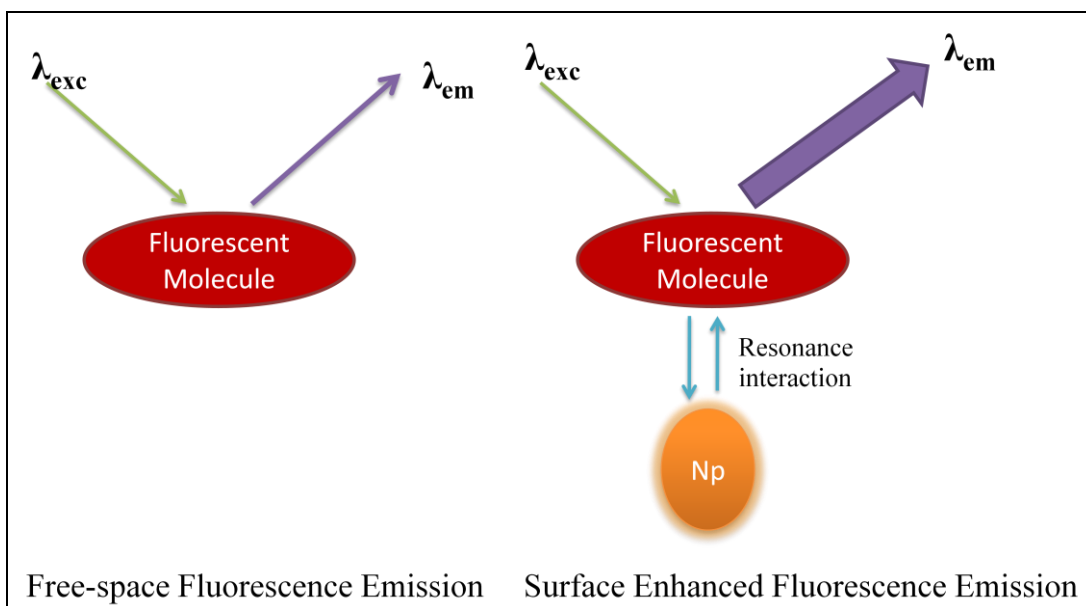


Figure 1.7 Schematic representations of fluorescence and surface enhanced fluorescence (Np: Nanoparticle).

In order to understand complicated interaction between metal nanoparticle and fluorophore, related Maxwell's equations must be solved [28]. Here, the phenomena will be explained by showing the spectral changes.

There are two important concepts; quantum yield (Q_0) and life time (τ). Quantum yield can be defined as the ratio of number of molecules that fluoresce (photons emitted) to the total number of excited molecules (photons absorbed). Life time is defined as the time that molecule spend at excited state before emission [29].

In a regular fluorescence mechanism, a fluorophore absorbs light and is excited to the singlet state (S_1) and emits light with a certain rate (radiative rate constant, k_f). As excited molecule returns ground state, some non-radiative steps may occur (e.g. intersystem crossing, external conversion, and internal conversion), the rate constant of all non-radiative processes can be represented as k_{nr} .

Quantum yield (Equation 1) and life time (Equation 2) can be represented as;

$$Q_0 = \frac{k_f}{k_f + k_{nr}} \quad (\text{Equation 1})$$

$$\tau_0 = \frac{1}{k_f + k_{nr}} \quad (\text{Equation 2})$$

The radiative rate constant (k_f) mainly depends on the chemical structure of the molecule. On the other hand most of non-radiative steps are strongly related to environment of the molecule [30, 31].

The intensity of fluorescence decreases as fraction of radiationless processes increase. This intensity decrease is called “quenching” [32]. Typical quenching processes are; collisional quenching, static quenching, Förster resonance energy transfer (FRET).

Resonance energy transfer occurs if two molecules are situated close to each other and the emission spectrum of one molecule (donor) overlaps with absorption spectrum of other molecule (acceptor). If both molecules have fluorescent property, then FRET enforces the emission intensity of the acceptor. Efficiency of energy transfer depends on distance between the molecules which is called as Förster distance (< 5 nm). FRET can be used as a “spectroscopic ruler” to measure the distance between the sites of proteins. In the case of surface enhanced fluorescence (SEF) studies, the donor is a fluorescent molecule and acceptor is a metal nanoparticle. If they are placed closer than Förster resonance energy distance, the emission intensity of fluorescent molecule is quenched due to energy transfer from fluorophore to the metal nanoparticles [32].

When a metal nanoparticle is placed at a certain distance ($>$ Förster distance) to the fluorophores, the presence of surface plasmons around metal nanoparticles can alter the conditions since metal nanoparticles provide additional electromagnetic field (E_m).

Metal nanoparticles amplify the incident light field and increase the radiative rate. Therefore when the fluorophore is in close proximity to metal nanoparticles, quantum yield and life time changes as follows [33];

$$Q_m = \frac{k_f + k_m}{k_f + k_{nr} + k_m} \quad (\text{Equation 4})$$

$$\tau_0 = \frac{1}{k_f + k_{nr} + k_m} \quad (\text{Equation 5})$$

Presence of metal nanoparticles increase the quantum yield ($Q_m > Q_0$) and decrease the life time ($\tau_m < \tau_0$).

The quantum yield of rhodamine B and rose bengal are 0.48 and 0.02, respectively. The emission intensity of rhodamine B and rose bengal close to silver island films were studied by Lakowicz *et al.* [34]. He found that the emission intensity of rhodamine B was increased 1.2-fold and Rose Bengal was increased 4.8-fold in the presence of silver island films.

Since fluorescence of fluorophores with high quantum yield is already an efficient process, the electromagnetic effect of low quantum yield fluorophores will be higher.

The effect of metal nanoparticles on the Jablonski diagram of fluorescence can be seen in Figure 1.8.

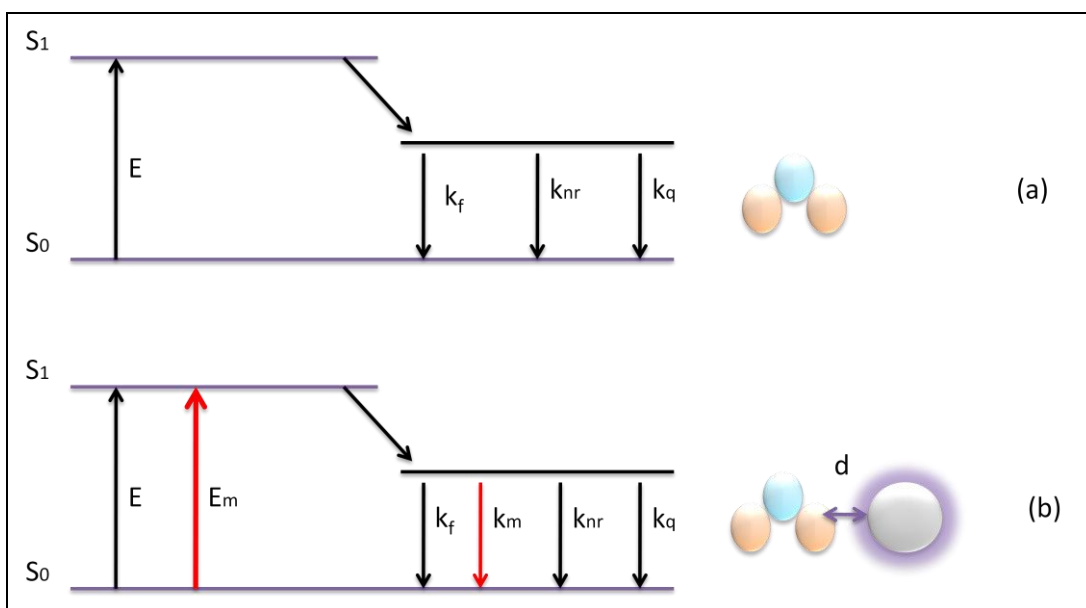


Figure 1.8 Jablonski diagram (a) fluorophore alone, (b) fluorophore located near metal nanoparticle.

In order to obtain the highest enhancement factor, two conditions must be satisfied:

- 1- The metal nanoparticles and fluorophores must be in resonance interaction. That is, the frequency of surface plasmons should overlap with the emission frequency of fluorophore. Since surface plasmon frequency depends on size and shape of the metal nanoparticles whereas emission wavelength of fluorophore is characteristic and cannot be changed [35], the shape and size of metal nanoparticles should be tuned to get a higher enhancement factor. A shift in the plasmon frequency of gold nanoparticles due to size changes can be seen in Figure 1.9.

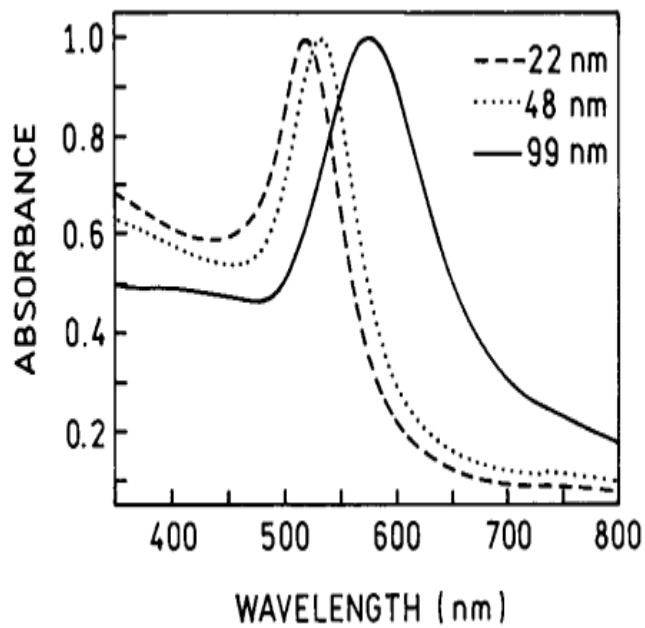


Figure 1.9 Plasmon absorption of spherical gold nanoparticles with different sizes [36].

- 2- Distance between metal nanoparticle and fluorophore must be precisely controlled. Otherwise, non radiative energy transfer (Förster transfer) occurs from fluorophore to metal nanoparticles and it leads to quenching [36, 37]

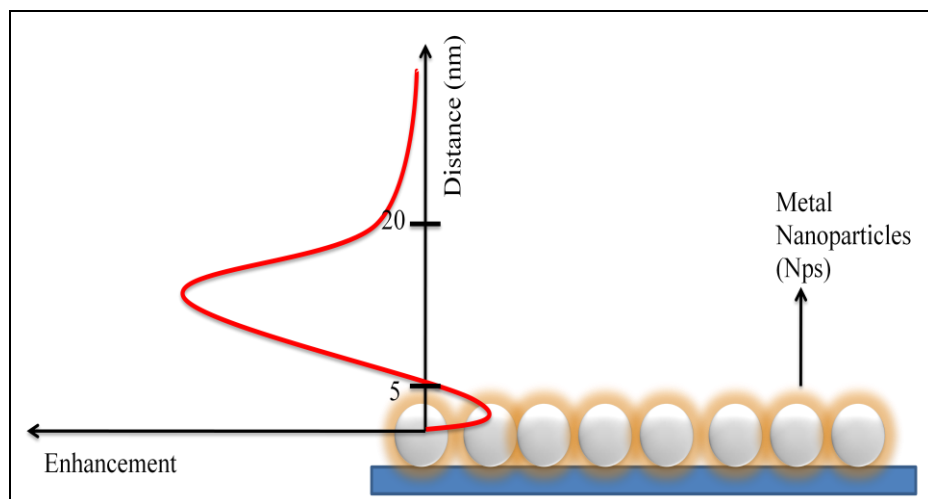


Figure 1.10 The effect of distance to enhancement.

Experimental studies have shown that there are two results pertaining to the optimal distance range for maximum enhancement. Some results show that 40 to 60 nm distances provides highest enhancement and there is a second maximum point when the distance is 10 nm [38-40]. However, the optimum range is found as 5 to 20 nm

(Figure 1.10) in most of the studies. If the distance is less than 5 nm, quenching occurs. Enhancement is obtained between 5 to 20 nm. If the distance is more than 20 nm, fluorescence mechanism is not affected because there is no interaction between fluorophore and metal nanoparticle [24, 41-44]. The effect of distance between fluorophores and metal nanoparticle on enhancement is shown in Figure 1.10.

Controlling the distance is the most difficult task in SEF studies. It can be provided either by attaching a molecule to the fluorophore or forming a spacer (distance layer) between metal nanoparticles and fluorophores.

Polymer film [38], oxide layer [40] or fatty acid layer [44] have been used as a spacer layer. Polymer film, oxide and fatty acid layer can be formed by applying spin coating, Langmuir-Blodgett, vapor deposition techniques, respectively [45].

The spacer material used must be transparent to incident light, dielectric and nonreactive with fluorophore and metal nanoparticles.

In conclusion, and ideal conditions for SEF is stated below;

1- Metal nanoparticles coated surface:

The distribution of metal nanoparticles on the surface must be homogenous in order to have reproducible enhancement. The plasmon absorption of nanoparticles must be intense. The shape and size of the metal nanoparticle must be tuned to provide overlapping of plasmon absorption and emission of fluorophore.

2- Spacer layer on metal nanoparticles:

The layer must be uniformly formed over metal nanoparticles with precisely controlled thickness.

1.4.2.4 Applications of Surface Enhanced Fluorescence (SEF)

Fluorescence became an indispensable technique in recent years due to its high sensitivity. Despite its high sensitivity however, advances in technology always ask for lower detection limits.

Surface enhanced fluorescence (SEF) phenomena have potential to be used in most of the fluorescence applications where increasing the sensitivity of the method is required by amplifying the signal of emission.

In drug research and DNA analysis (DNA hybridization and sequencing), assays can be coated with silver nanoparticles and the lightening effect of nanoparticles would increase the fluorescence of fluorophore specifically bound to DNA.

Metal nanoparticles could be used for the detection of fluorophores with low quantum yield by means of SEF phenomena.

1.4.2.5 Recent Studies on SEF and Enhancement Factors (EF) achieved

In Table 1.1 some research articles selected and the components of SEF assays; metal nanoparticle, fluorophore, spacer and their properties and achieved enhancement factor are summarized.

Table 1.1 List of recent surface enhanced fluorescence studies.

Metal Type	Metal Nanoparticle Size (nm)	Plasmon Absorption (nm)	Spacer or Linker Type	Spacer Thickness (nm)	Fluorophore Type	Fluorophore Emission (nm)	Enhancement Factor	Reference No
Ag	20-80	450	BSA	NA	Texas Red	620	8.6	[46]
Ag	20-80	450	BSA	NA	Fluorescein	520	12.8	[46]
Ag	35	440	BSA		Fluorescein	525	5	[46]
Au	123	850	BSA		ICG	850	50	[47]
Au	80	530	BSA		DP	620	5.7	[48]
Ag	10-40, 100-300	440, 550	HSA		ICG	830	10 and 50	[49]
Ag	> 50	430	HSA		ICG	830	30	[50]
Ag	10 (layer)	NA	IgG and Silica	10	FITC	530	8	[51]
Ag	20	439, 800	PSS (LB*)	NA	R123	546	~10	[52], [53]
Ag	20	439, 800	PDAC (LB)	NA	SRB	597	~10	[52], [53]
Fe	1 (film)	NA	NA	NA	Fluorescein	520	9	[54]
Fe	1 (film)	NA	NA	NA	Acridine Orange	543	3,8	[54]
Ni	NA	300-800	NA	NA	Rhodamine 101	530	1,5	[55]
Ni	NA	300-800	NA	NA	IR 792	820	2,5	[55]
Ag	20	430-440	Silica (PVD**)	10	CdSe/ZnS	506	15,1 and 21.6	[56]
Au	40	NA	Silica(PVD)	50	Cy5	660	3,8	[57]

Metal Type	Metal Nanoparticle Size (nm)	Plasmon Absorption (nm)	/Spacer or Linker Type	Spacer Thickness (nm)	Fluorophore Type	Fluorophore Emission (nm)	Enhancement Factor	Reference No
Ag	NA	460	Stearic acid (LB)	10	SRB	585	10	[58]
Ag on PB	40 - 50	600-700	BSA	NA	Cy5	660	8	[59]
Ag	6	570	Alumina	10	Rhodamine B	580	10	[60]
Ag	6	507	NA	6	OD-PTCO	688	20	[61]
Ag	14	610	NA	6	OD-PTCO	688	10	[61]
Au	30	530	Silica	5	Ru(dpp)3	612	5	[62]
Ag	30-80	420	HSA	4	FITC	525	~10	[63]
Ag	70	370	PSS/PDADMAC (LB)	15-20	Rhodamine 6G	~590	5 to 30	[64]
Au	30	NA	Silica	25	CYe	NA	6,8	[65]
Ag	46	NA	Silica	24	CYe	NA	12,5	[65]
Cu	3	NA	NA	0	Acridine Orange	543	2,5	[66]

* LB : Langmuir-Blodgett

** PVD: Physical Vapor Deposition

According to Table 1.1, silver or gold nanoparticles are chosen in most of the studies due to their high plasmon effect. Immersion of slide to the colloid mixture, physical techniques (i. e. evaporation) and electrochemical methods are usually applied for the deposition of nanoparticles onto slides.

When recent studies were investigated, forming a spacer between fluorophore and metal nanoparticles has been still the major problem to be solved. The distance is provided either by a big biological molecule linked to fluorophores (Proteins; BSA, HSA) or a spacer layer. Linker molecules provide both distance and adhesion of fluorophores to the surface of nanoparticles. The chemical binding between linker molecule and fluorophore is maintained by wet chemical procedures [46-49, 63]. Silica, alumina, stearic acid are the examples of spacer layer that are used and physical deposition techniques (sputtering, evaporation), Langmuir-Blodgett film system and spin coating are applied for the deposition of spacer layers mentioned [51-53, 56, 57, 64, 65]. Obtained enhancement factors are varied between 2.5 to 50 but usually concentrated around 10. As our conclusion from the publications, enhancement factor in the range of 0-30 can be achieved if the spacer thickness is in the range of 0-20 nm provided.

1.5 Thin Film Deposition Techniques

1.5.1 Physical Vapor Deposition (PVD)

Physical vapor deposition (PVD) is a technique for the deposition of thin films at atomic level. Typical PVD process involves [67]:

- Vaporization of material that will be deposited.
- Transportation of vapor to the substrate in low pressure medium.
- Condensation of vapor on substrate.

Deposition of films with thicknesses ranging from a few nanometers to thousands of nanometers is possible by applying PVD [67]. The deposition rate can vary between 10- 100 Angstrom per second. The most widely used PVD methods are:

Thermal evaporation: The source material is heated by electrical resistance under low vacuum [68].

Electron beam: The source material is heated by electron bombardment under high vacuum [68].

Sputtering: Highly energetic atoms or ions hit the source material and sputter atoms from the surface. The sputtered atoms condense on substrate [69].

1.5.2 Langmuir-Blodgett (LB) Film Formation

Langmuir-Blodgett films were first applied by Irvin Langmuir and Katharina Blodgett in 1917 and 1935, respectively. It was found that when fatty acids were spread over water, a molecular monolayer was formed at water air interfaces with perpendicular orientation of molecules due to their amphiphilic properties. [70]

Monolayer can be maintained in condensed and stable state by controlling the temperature and surface pressure of monolayer [71].

It is possible to control the area per molecule of monolayer by barriers positioned as touching the surface of water. Compression by moving barriers provides pressure-area relationship. The monolayer can be packed until a certain surface pressure and transferred to solid substrate. Different deposition types are possible by changing the initial conditions.

The LB film is characterized by transfer ratio (deposition ratio). Transfer ratio is defined as ratio of the area decrease of monolayer to the area of substrate coated. If asymmetric compression is applied, transfer ratio is expected to be close to unity [70].

1.6 Aim of the Study

The role and importance of spacer in surface enhanced fluorescence applications has been understood. The objective is to construct surface enhanced fluorescence (SEF) substrates that are stable and providing high enhancement factors. Therefore, the effect of thickness and material of spacer will be studied. Different techniques (physical vapor deposition, sol-gel and Langmuir-Blodgett) will be applied in order to find spacer with high performance.

CHAPTER 2

EXPERIMENTAL

2.1 Chemical and Reagents

- i. **De-ionized water:** Provided from Elix 5, Millipore water purification system.
- ii. **Silver nitrate:** AgNO_3 , $\geq 99.0\%$, from Sigma-Aldrich.
- iii. **Gold (III) chloride trihydrate:** $\text{HAuCl}_4 \cdot 3\text{H}_2\text{O}$, $\geq 99.0\%$, from Sigma-Aldrich. 0.1 M aqueous solution was prepared as stock and used for all experiments.
- iv. **Sodium citrate tribasic dihydrate:** $\text{Na}_3\text{C}_6\text{H}_5\text{O}_7 \cdot 2\text{H}_2\text{O}$, $\geq 99.0\%$, from Sigma-Aldrich, 1.0% (w/v) aqueous solution was prepared freshly just before the experiments.
- v. **(3-Aminopropyl)triethoxysilane (APTES):** $\text{H}_2\text{N}(\text{CH}_2)_3\text{Si}(\text{OC}_2\text{H}_5)_3$, $\geq 99.0\%$, from Fluka. 1.0% (w/v) aqueous solution was prepared for all experiments.
- vi. **Rhodamine B:** $\text{C}_{28}\text{H}_{31}\text{ClN}_2\text{O}_3$, from Merck KGaA, 10^{-4} M aqueous solution was prepared as stock.
- vii. **Fluorescein:** $\text{C}_{20}\text{H}_{12}\text{O}_5$, from Merck KGaA.
- viii. **Rhodamine 6G:** $\text{C}_{28}\text{H}_{31}\text{N}_2\text{O}_3\text{Cl}$, from Sigma-Aldrich.
- ix. **Acridine Orange:** $\text{C}_{17}\text{H}_{19}\text{N}_3 \cdot \text{HCl} \cdot x\text{H}_2\text{O}$, 99% from Sigma-Aldrich, 10^{-4} M aqueous solution was prepared as stock.
- x. **Acetone:** $\text{C}_2\text{H}_6\text{O}$, $\geq 99\%$ from Sigma-Aldrich.
- xi. **Ethanol:** $\text{C}_2\text{H}_5\text{OH}$, absolute for analysis, from Merck KGaA.
- xii. **Tetraethoxysilane (TEOS):** $\text{SiC}_8\text{H}_{20}\text{O}_4$, 98% from Sigma-Aldrich.
- xiii. **Nitric acid:** HNO_3 , 65% for analysis, from Merck KGaA.

- xiv. **Hydrochloric acid:** HCl, 36.5-38.0%, from Sigma-Aldrich
- xv. **Brilliant Cresyl Blue (BCB):** $C_{17}H_{20}ClN_3O \cdot 0.5ZnCl_2$, dye content 65% from Sigma-Aldrich.
- xvi. **Chloroform:** $CHCl_3$, 99-99.4%, stabilized with 1% ethanol from Riedel de Haen.
- xvii. **Stearic acid:** $CH_3(CH_2)_{16}COOH$, $\geq 99\%$, from Merck KGaA.

2.2 Instrumentation

2.2.1 Fluorescence Spectrometer

LS 50B fluorescence spectrometer manufactured by Perkin Elmer, USA equipped with a xenon lamp and photomultiplier detector was used for the emission and excitation measurements of fluorescence dyes. A standard fluorometer quartz cell with 10 mm path length was used for the fluorescence measurements of solutions (Figure 2.1.a). Front-face sample geometry was used for surface enhanced fluorescence of the dyes (Figure 2.1.b).

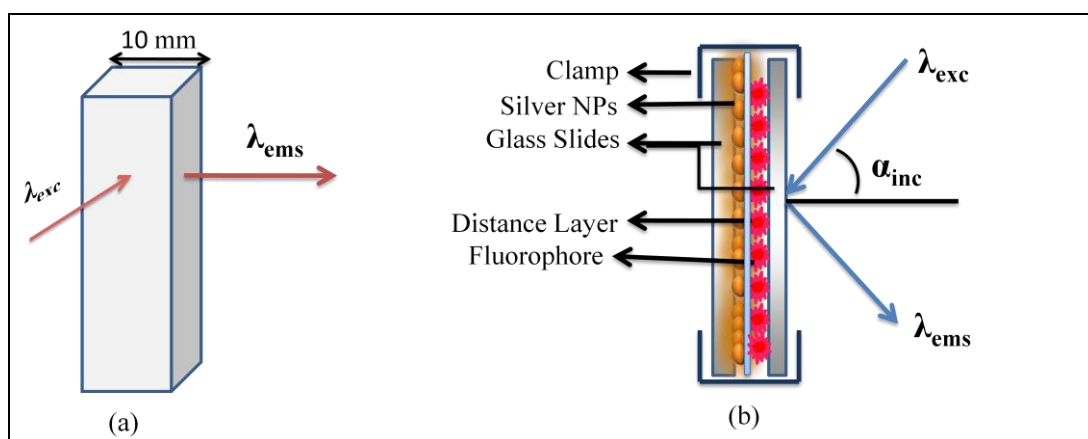


Figure 2.1 Sample geometry of fluorescence measurements for (a) solution (b) surface enhanced fluorescence.

A homemade stand (Figure 2.2) was designed in order to find the optimum incident light angle (α_{inc}). Cuvette holder was removed and a bottom of Petri dish was fixed

instead of it. Top cover of Petri dish was divided into degree portions as each movement of portion changes the incident angle 15° .

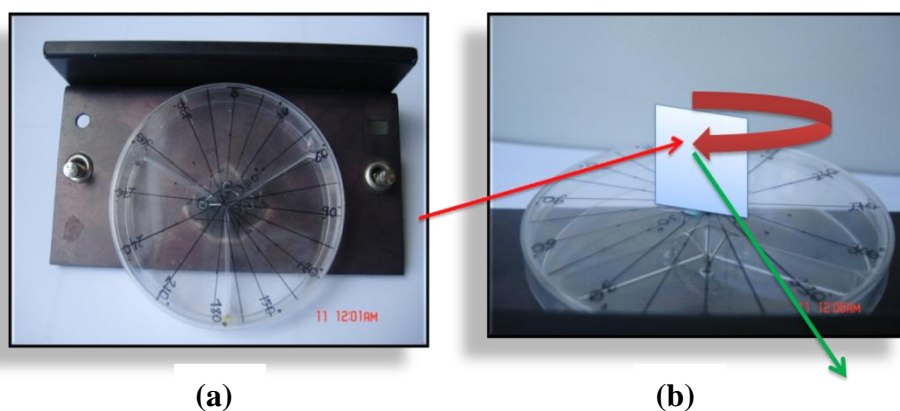


Figure 2.2 Homemade stand for incident light angle optimization, (a) top, (b) front view.

2.2.2 UV-VIS Spectrometer

T80 double beam spectrometer manufactured by PG Instruments, UK equipped with socket deuterium and tungsten halogen lamp and multiplier detector was used in order to observe the optical properties of gold and silver nanoparticles.

2.2.3 Centrifuge

NF 200 centrifuge manufactured by NÜVE, Turkey with maximum 5000 rpm rotating speed and was used to separate and concentrate the nanoparticles in colloid solution.

2.2.4 Surface Enhanced Raman Spectrometer (SERS)

LabRAM HR Raman spectrometer manufactured by Jobin Yvon Horiba, France equipped with a charged-coupled device (CCD) detector and holographic notch filter was used for surface enhanced Raman scattering spectrum (SERS) studies of Brilliant Cresyl Blue.



Figure 2.3 Raman spectroscopy [67]

2.2.5 Field Emission Scanning Electron Microscopy (FE-SEM)

Quanta 400 F field emission scanning electron microscopy (FE-SEM) from FEI Company, the Netherlands was used for the shape and size characterization of nanoparticles, at METU Central Laboratory.

2.2.6 Physical Vapor Deposition System (by Sputtering Method)

NanoD-Sputter physical vapor deposition system manufactured by Vaksis, Turkey (Figure 2.3) was used to deposit nanosize thin films of silica and zinc oxide onto silver nanoparticle coated surface of glass slides.



Figure 2.4 Sputtering system [68].

2.2.7 Physical Vapor Deposition System (by Evaporation Method)

A homemade thermal evaporator built by Physics Department, METU, was used for the deposition of gold film with 10 nm thickness onto surfaces of silver nanoparticle coated and bare glass slides.

2.2.8 Langmuir-Blodgett Film Formation System

Minimicro Langmuir-Blodgett (LB) film formation system manufactured by KSV (Figure 2.5), Finland was used. The system mainly consists of a servo-controlled dipper motor, a PTFE trough, platinum Wilhelmy plate hooked to a balance and movable barriers.



Figure 2.5 Langmuir-Blodgett film formation system [69].

2.3 Preparation of Nanoparticles

2.3.1 Silver Colloid

Silver colloid was prepared by applying chemical reduction method [70]. 90 mg of AgNO_3 were added to 500 ml of de-ionized H_2O . The solution was heated until boiling and kept stirred. 1% (w/v) of $\text{Na}_3\text{C}_6\text{H}_5\text{O}_7$ aqueous solution was prepared. Different amount of 1% $\text{Na}_3\text{C}_6\text{H}_5\text{O}_7$ solution was added to boiling AgNO_3 solution. After color of the final solution was changed to pale yellow, it was kept heated and stirred for one more hour.

2.3.2 Gold Colloid

Gold colloid was prepared by chemical reduction method [70]. 100 ml of 0.01% (w/v) HAuCl_4 aqueous solution was prepared and heated until boiling and stirred constantly. Freshly prepared 1ml of 1% (w/v) $\text{Na}_3\text{C}_6\text{H}_5\text{O}_7$ aqueous solution was added to the boiling solution. After an immediate color change to the dark red, the final solution was kept heated for another 5 minutes.

2.3.3 Silica Coated Silver Colloid

Silica coating of silver colloid was performed by following optimized Stöber method [71] in our laboratory.

Basically the method consists of sol-gel formation using tetraethyl orthosilicate (TEOS) as precursor under the catalytic action of ammonia in ethanol/H₂O mixture that contains silver nanoparticles.

2.4 Preparation of Fluorescence Solutions

Aqueous solutions of 10⁻⁴ M rhodamine B and fluorescein were prepared for fluorescence measurements and used as stock solutions. Emission of fluorescein is pH sensitive; therefore the pH of the solution was set 10 by addition of 3 M NaOH.

2.5 Preparation of Glass Slides

Standard microscope glass slides were cut into 25.0×7.0 mm dimensions with the help of a diamond tipped glass cutter

2.5.1 Cleaning of Slides

Prior to use of glass slides, a multi step cleaning procedure was applied to the glass slides. First slides cleaned in a warm solution of mild liquid detergent and water. Then they were kept in acetone for 15 minutes at 50 °C. After flushing with ethanol and rinsed with de-ionized water 3 times, they were stored in 33% (v/v) HNO₃ solution until use. The slides were rinsed with de-ionized water for 3 times again and dried with N₂ gas prior to the derivatization.

2.5.2 Etching the Slides

The slides were kept in 10% (v/v) HF solution for 15 minutes in order to create cavities on the surface. Afterwards substrates were rinsed for 3 times with de-ionized water and dried with stream of N₂ gas

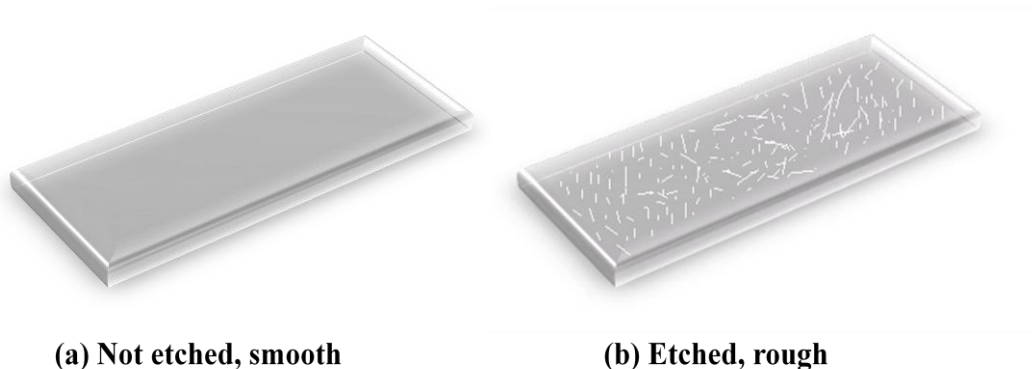


Figure 2.6 Schematic representation of (a) not etched and (b) etched surface

2.5.3 Derivatization (Modification) of the Slides

Each substrate (25.0×7.0 mm) were immersed into 1% (v/v) APTES solution for 0.5, 1.0, 3.0 hours [72]. Following derivatization, the substrates were rinsed with de-ionized water and dried under the stream of N₂ gas.

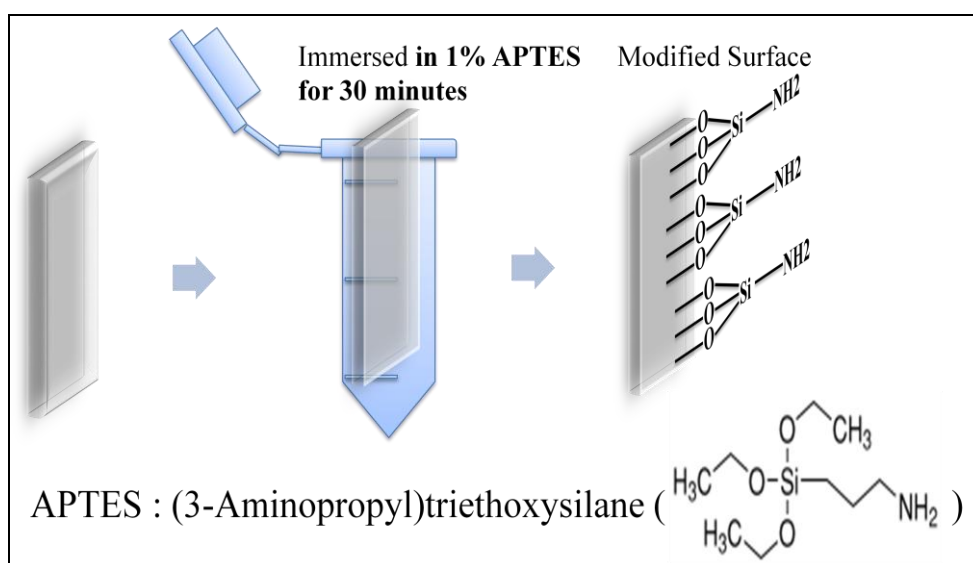


Figure 2.7 Schematic representation of surface derivatization.

2.6 Deposition of Metal Nanoparticles onto Derivatized (Modified) Slides

Tubes (1.5 ml) were filled with gold and silver colloid (prepared at 2.3.1 and 2.3.2 respectively). Then modified slides (after the procedure given at 2.5.3) were placed and kept inside the tubes for 1 to 24 hours.

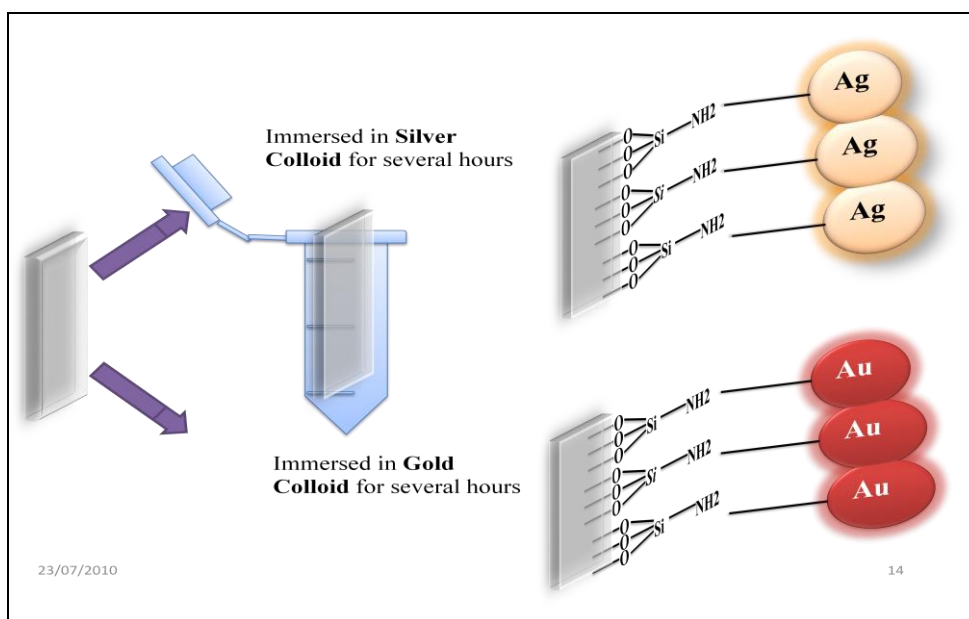


Figure 2.8 Deposition of metal nanoparticles on modified slide by immersion method.

The slides were taken out of the tubes and cleaned by de-ionized water in order to remove excess and unbound metal nanoparticles. Finally, the slides were dried by N₂ gas.

During storage, slides were kept in dessicator at dark to prevent oxidation and photodecomposition of metal nanoparticles. Whenever the lid of the dessicator was removed, it was purged with N₂ for 5 minutes just after the lid was closed

2.7 Deposition of Spacer (Distance Layer) onto Metal Nanoparticle Coated Slides

Three different methods were used for the deposition of spacer.

2.7.1 Physical Vapor Deposition of Silica and Zinc oxide Layers by Sputtering

Metal nanoparticles coated substrates were placed on sample holder of the sputter. During the placement of the substrates, care should be taken not to cause any contamination on the surface. Therefore clean gloves, stainless steel tweezers were used and placement was done under laminar flow cabinet.

The sample holder was installed inside the chamber and the door of the chamber was closed tightly. The chamber pressure was set to 5×10^{-6} Torr. When the pressure was achieved, argon gas was released and final pressure was set to 4×10^{-3} Torr. The power of the RF generator was increased 5 watts/min to 200 Watts. Another 15 minutes passed for the stabilization of source. The shutter between the source and substrates was opened and deposition of silica or zinc oxide was started. During the deposition, the sample holder was rotated with 10 rpm by means of a stepper motor to provide thickness homogeneity of the film.

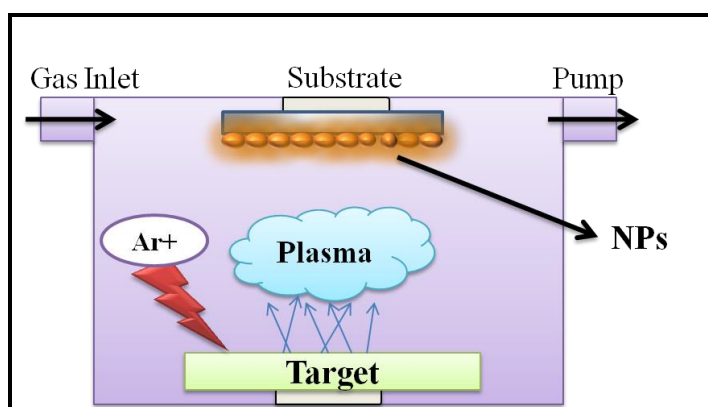


Figure 2.9 Sputtering system (Inside the chamber).

2.7.2 Physical Vapor Deposition of Gold by Thermal Evaporation

As stated in 2.7.1, clean tools were used while handling and placing the slides on the sample holder. Sample holder containing the glass slides (silver nanoparticles coated and bare) was installed inside the chamber. Gold foil (99.999%, 5N) was placed inside a tungsten boat. The two sides of the tungsten boat were attached to the electric resistance heater probes in order to heat up the target material (gold foil). The pressure of the chamber was decreased to 5×10^{-6} Torr by means of turbo pumps.

After desired pressure achieved, the tungsten boat was heated, the shutter was open and deposition of gold nanofilm started.

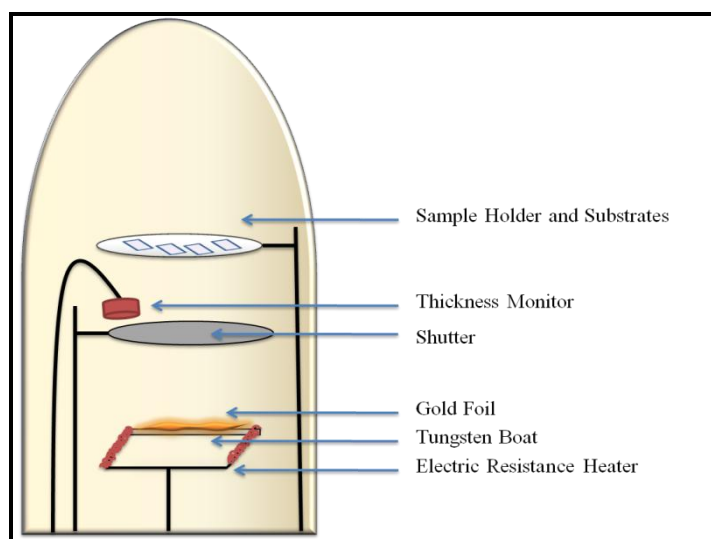


Figure 2.10: Thermal evaporation system.

2.7.3 Formation of Stearic Acid Molecular Layers by Langmuir-Blodgett Film System

2.7.3.1 Cleaning and Preparation of Langmuir-Blodgett Film System

Prior to formation and deposition of layers with the Langmuir-Blodgett (LB) film system, cleaning was done carefully according to procedures set and recommended by the manufacturer, as even the smallest amount of contamination is not tolerable in either film formation or deposition. The PTFE trough and movable Delrin barriers were cleaned first by pure ethanol and then de-ionized water. The balance and dipper were placed at the center of the trough. The trough was filled with de-ionized water until the water level was 2 mm above the trough edges. Platinum Wilhelmy plate was cleaned in given order with acetone, ethanol and de-ionized water to remove any organic contamination. Wilhelmy plate was hanged to the balance hook and the balance vertical position was adjusted so that two-thirds of the plate was immersed in the aqueous subphase.

2.7.3.2 Isotherm Measurements

The position of the barriers was set to zero when they were at the outer limits of the trough and then symmetric compression with the barriers was started. If the balance reading was less than 0.3 mN/m during the compression process up until when the barriers were closest to each other, the wetted components were accepted to be clean enough for the purpose of stearic acid monolayer formation and deposition. If the reading exceeded 0.3 mN/m, aforementioned cleaning procedures were repeated. The balance reading and barrier positions were zeroed again prior to placement of the surfactant solution onto the subphase. Freshly prepared 1 mg/ml (w/v) stearic acid (surfactant) solution in chloroform was used. The micro syringe used for placement of surfactant solution was first rinsed with chloroform 3 times. Approximately 20 μl of surfactant solution were pulled into the syringe. Droplets of surfactant solution formed on the syringe needle tip were placed gently on the surface of subphase. Letting the drops fall from a height instead of just making them contact the subphase could result in the surfactant molecules entering the subphase instead of spreading on the surface. The surface pressure value should not exceed 0.5 mN/m during the placement and spreading of the surfactant molecules. At least 10 minutes were allowed to pass for the chloroform to evaporate. The starting mean molecular area per stearic acid molecule was automatically calculated in the system software using the values of trough area, concentration of the stearic acid solution and the actual solution volume placed on the subphase, along with the surfactant molecular weight.

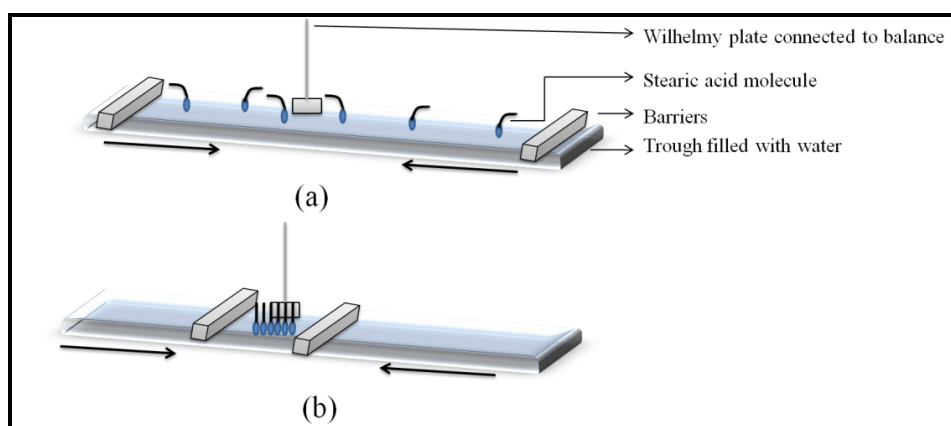


Figure 2.11 Isotherm experiment (Compression of Langmuir Monolayer), (a) stearic acid monolayer in “gaseous phase” (b) stearic acid monolayer in “solid phase”.

For the isotherm experiment the compression rate and target surface pressure was set as 5 mm/min. and 60 mN/m, respectively. Surface pressure vs. mean molecular area per stearic acid molecule (π -A) isotherm measurement was initialized and controlled via the system software (Figure 2.11). As results of the isotherm experiment, “phase transitions” of the stearic acid monolayer on aqueous subphase were observed including the “solid phase” (Figure 2.11.b) and the surface pressure and mean molecular area per stearic acid molecule values at which these “transitions” occur were obtained.

2.7.3.3 Dipping (Coating) Experiments

System cleaning described in section 2.7.3.1 was repeated after the isotherm experiment prior to the deposition of stearic acid monolayer onto surfaces. Silver nanoparticle coated substrate (25.0×7.0 mm glass slide) was attached to the dipper arm and immersed into the subphase prior to spreading of the surfactant. The reason for this was that as the substrate surface was hydrophilic, the deposition of the first layer of stearic acid molecules would happen at the hydrophilic “head” end of the surfactant as the substrate was raised from the subphase and through the spread monolayer. Approximately 20 μ l of surfactant solution were placed carefully onto the subphase and 10 minutes were allowed to pass for the chloroform to evaporate (Figure 2.9.a). For the calculation of transfer ratio (TR) the dimensions of the substrate was taken as 20.0×7.0×1.0 mm (height, width, thickness).

For the deposition of the monolayers, firstly the spread surfactant molecules were compressed until the surface pressure reached the target value. The optimum surface pressure value for deposition chosen by observing the previously obtained isotherm was set as the target pressure. Once this value was reached, 5 minutes were given for stabilization as the barriers made minute inward and outward movements for keeping the surface pressure constant at set target. Following this stabilization step, the upstroke movement of the dipper started and raised the substrate out of the subphase (Figure 2.12.b). When the substrate was pulled out of the liquid completely (no interaction with the subphase), the first monolayer was formed on the substrate surface (Figure 2.12.b). The substrate surface must be dried before the deposition of a second stearic acid monolayer, so a drying time of 20 minutes was allowed to pass after the formation of the first monolayer on the surface.

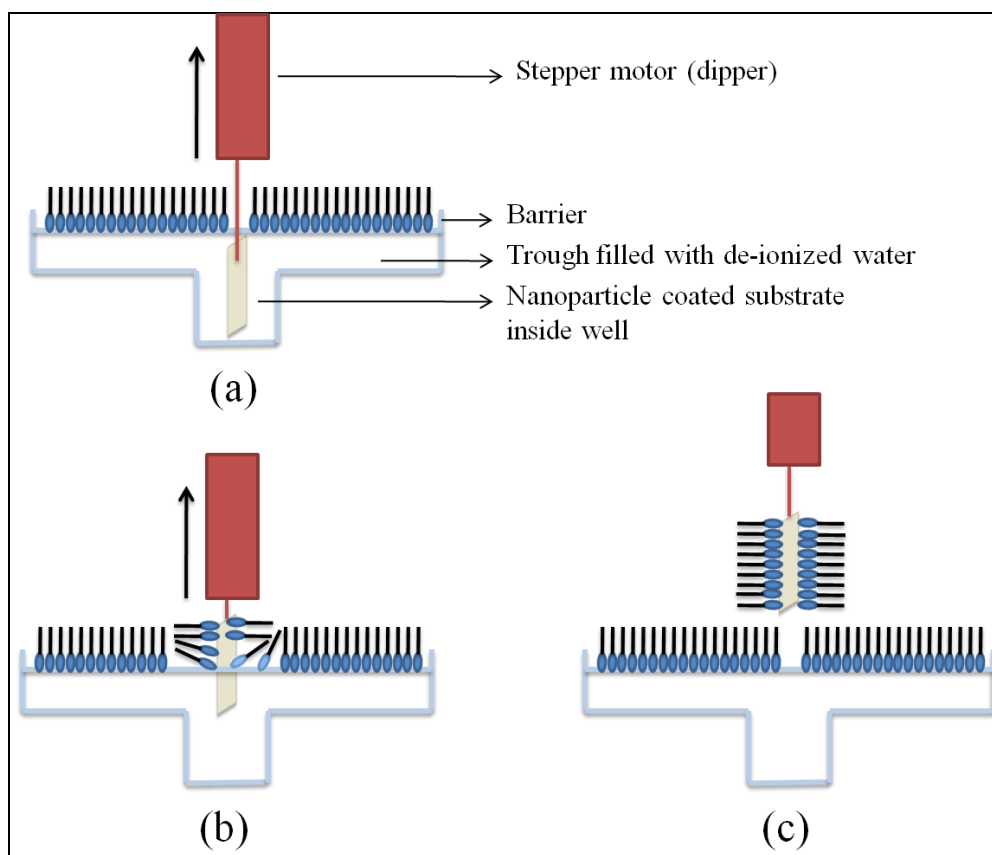


Figure 2.12 Dipping experiment.

Subsequent layers were formed in the same sequence as long as the stearic acid monolayer was maintained without collapsing, in other words the surface pressure being kept constant. The rate of upstroke and downstroke movements was set as 5 mm/min

Additional layers were deposited with resulting substrates ranging having 1 to 5 stearic acid layers.

2.8 Surface Enhanced Raman Scattering (SERS) Measurements

10 μl of 10^{-6} M brilliant cresyl blue (BCB) solution were dropped on the prepared substrate (metal nanoparticles coated surface). The measurement was performed before the drop dried. 10X objective lens was chosen and the exposure time was set to 1 second. The SERS intensities of BCB on nanoparticles coated and bare glass were compared.

CHAPTER 3

RESULTS AND DISCUSSION

SEF experiments were conducted both in solution and on prepared SEF substrates. Gold, silver and silica coated silver colloid were mixed with rhodamine B and fluorescein solution in order to observe emission enhancement.

SEF substrates consisted of spacer layer and silver nanoparticles were prepared. Silica, zinc oxide, gold and stearic acid layer was deposited onto silver nanoparticle coated surface by means of 3 different deposition techniques. Physical vapor deposition, sol-gel, silica, zinc oxide and gold layer were deposited by physical vapor deposition technique. Sol-gel method was also applied to coat the silver nanoparticles with silica layer in colloid mixture. Stearic acid layer was deposited by Langmuir- Blodgett system. The SEF substrates prepared in this work were given in Table 3.1

Table 3.1 The components of prepared SEF substrates

No	Metal Type	Spacer Type	Deposition Technique
1	Ag	Silica	Sputtering
2	Ag	Silica	Sol-gel
3	Ag	Zinc oxide	Sputtering
4	Ag	Gold	Thermal Evaporation
5	Ag	Stearic acid	Langmuir-Blodgett

The performance of the silica, zinc oxide, gold and stearic acid as a spacer layer was evaluated by considering the enhancement factors achieved. The effect of spacer

material and thickness on emission enhancement was investigated and thickness was optimized for maximum enhancement factor. SERS experiments were conducted for testing the stability and confirming plasmon effects of the nanoparticles.

3.1 Properties of Metal Nanoparticles

Silver and gold nanoparticles were prepared as described in sections 2.3.2 and 2.3.3, respectively. Physical appearance of colloidal solution was an initial indicator to show whether the nanoparticles were formed or not. Secondly, absorption spectrometry was used to monitor the plasmon absorption of nanoparticles. The correlation between surface plasmon resonance and morphology of the nanoparticles has been reported by Schultz S. *et al.* [73]. Field Emission Scanning Electron Microscopy (FE-SEM) was the most exact instrumentation utilized to observe shape and size of the nanoparticles prepared.

3.1.1 Silver Nanoparticles

The color of silver colloids is different than bulk silver particles. The appearance of the concentrated colloid system is turbid with a brownish color (Figure 3.1), consistent with the descriptions given in the literature [70].



Figure 3.1 Image of silver colloid.

Absorption spectrum (Figure 3.2) was obtained after 4-fold dilution of silver colloid with de-ionized water.

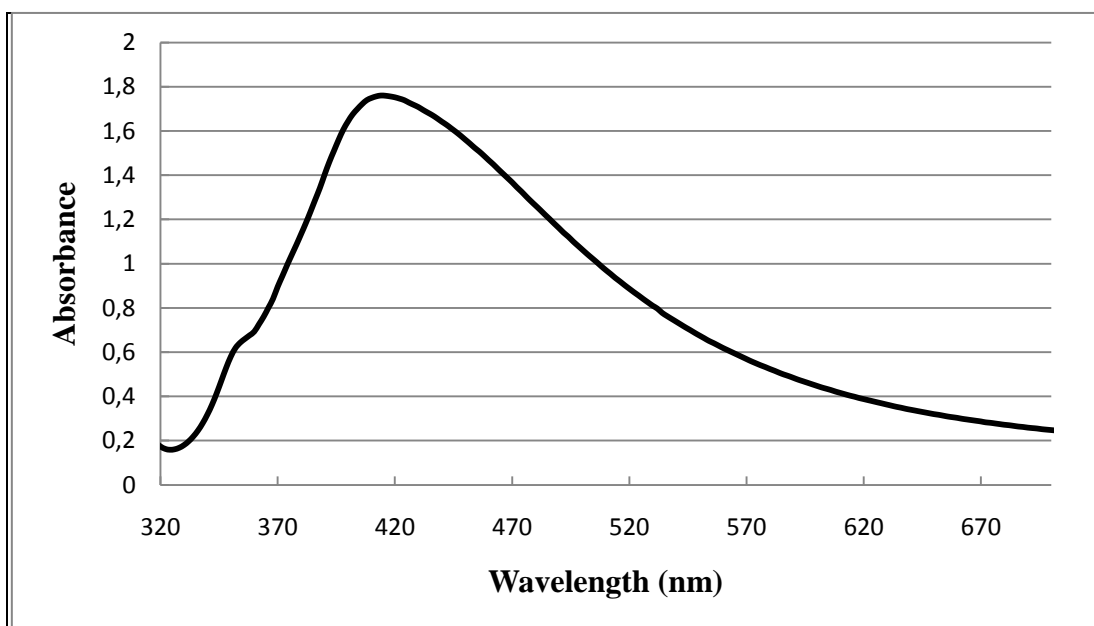


Figure 3.2 Absorption spectrum of silver colloid.

The spectrum had its maximum absorption signal intensity value 1.75 at 420 nm. According to previous studies, silver nanoparticles with size distribution of 60-80 nm and spherical shape shows maximum absorption around 410-440 nm.

Chemical reduction method (Section 2.3.1) is one of the most common and well-known method for the preparation of silver colloids in practice. However, the amount of $\text{Na}_3\text{C}_6\text{H}_5\text{O}_7$ aqueous solution differs between publications whereas the other parameters (boiling time, AgNO_3 concentration) are usually kept constant. An absorption spectrum with high intensity and a narrow band width was an indication of monodisperse nanoparticles formation with high plasmon efficiency. Therefore, the effect of $\text{Na}_3\text{C}_6\text{H}_5\text{O}_7$ aqueous solution was investigated in order to achieve monodisperse and high plasmon efficiency nanoparticles.

AgNO_3 solution was prepared as described in section 2.3.1. 10, 20, 30 and 40 ml of 1% (w/v) of $\text{Na}_3\text{C}_6\text{H}_5\text{O}_7$ aqueous solution were added to the boiling AgNO_3 solution.

It is expected that as the amount of 1% (w/v) $\text{Na}_3\text{C}_6\text{H}_5\text{O}_7$ aqueous solution added increases, the size of silver nanoparticles will decrease and it is known that the spectrum shifts longer wavelength as particle size increases [74].

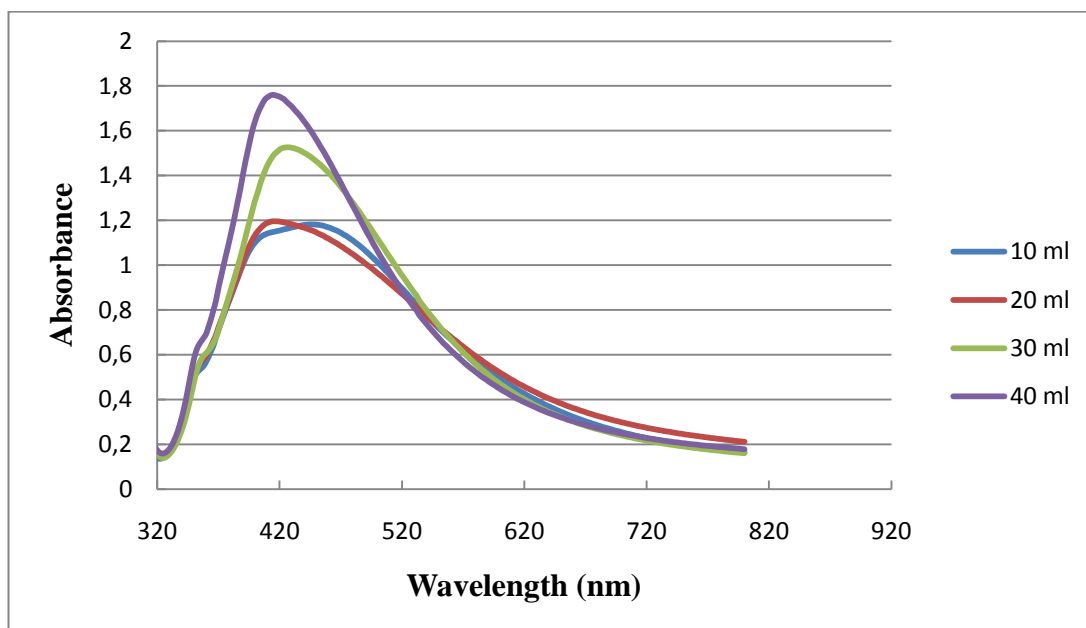


Figure 3.3 Absorption spectra of silver colloids, addition of different amount of 1% (w/v) of $\text{Na}_3\text{C}_6\text{H}_5\text{O}_7$ aqueous solution.

In Figure 3.3, a broader spectrum with maxima at 412 and 454 nm was obtained when 10 ml of 1% (w/v) of $\text{Na}_3\text{C}_6\text{H}_5\text{O}_7$ aqueous solution were added. The broader spectrum with two absorption peaks indicated formation of polydisperse silver colloidal solution with wires, rods and spherical nanoparticles. When the amount of 1% (w/v) of $\text{Na}_3\text{C}_6\text{H}_5\text{O}_7$ aqueous solution was increased to 20 ml, the maximum absorption shifted to blue region and plasmon band width became narrower. Addition of 30 ml and 40 ml of 1% (w/v) of $\text{Na}_3\text{C}_6\text{H}_5\text{O}_7$ aqueous solution did not cause any significant shift with respect to the spectrum of the nanoparticles prepared with addition of 20 ml of 1% (w/v) of $\text{Na}_3\text{C}_6\text{H}_5\text{O}_7$ aqueous solution. However maximum intensity of plasmon absorption was obtained with 40 ml of 1% (w/v) of $\text{Na}_3\text{C}_6\text{H}_5\text{O}_7$ aqueous solution was added. Therefore, the optimal 1% (w/v) of $\text{Na}_3\text{C}_6\text{H}_5\text{O}_7$ aqueous solution to be added to the AgNO_3 solution was determined to be 40 ml. The maximum absorption wavelength and corresponded amount of 1% (w/v) of $\text{Na}_3\text{C}_6\text{H}_5\text{O}_7$ aqueous solution were given in Table 3.2

Table 2.2 Maximum absorption wavelength (λ_{\max}) and amount of 1 % (w/v) of $\text{Na}_3\text{C}_6\text{H}_5\text{O}_7$ aqueous solution (V).

V (ml)	λ_{\max} (nm)
10	412, 454
20	412, 440
30	430
40	420

Physical appearance of the colloid or the obtained absorption spectra was not sufficient to define the exact morphology of silver nanoparticles. Therefore field emission scanning electron microscopy images were recorded.

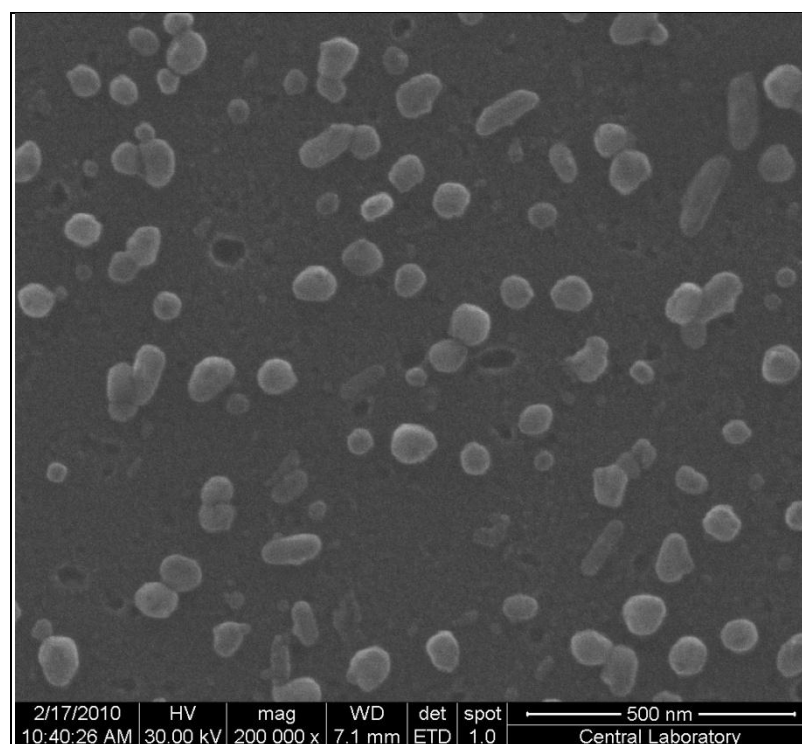


Figure 3.4 FE-SEM image of silver nanoparticles deposited on glass slide.

In Figure 3.4, it could be observed that, there were also a lower percentage of rod-shaped silver nanoparticles. Arithmetic average particle diameter of silver nanoparticles was calculated as 61.0 ± 11.2 nm from the FE-SEM images. Results showed that the silver nanoparticles prepared displayed expected properties.

3.1.2 Gold Nanoparticles

Like silver, gold colloid has a different color than its bulk form. Bulk form of gold has a dark shiny yellow color (which is named golden). On the other hand, gold colloidal systems exhibit color ranging from red to blue depending on the size and shape of the nanoparticles [17].

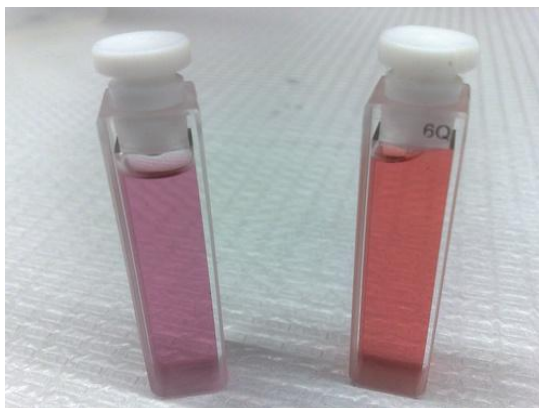


Figure 3.5 Image of gold colloid.

The gold colloid prepared as described in section 2.3.3 had red color (Figure 3.5). This physical appearance was in agreement with related publications [17]. The gold colloid was diluted 4-fold with de-ionized water prior to the absorption measurement.

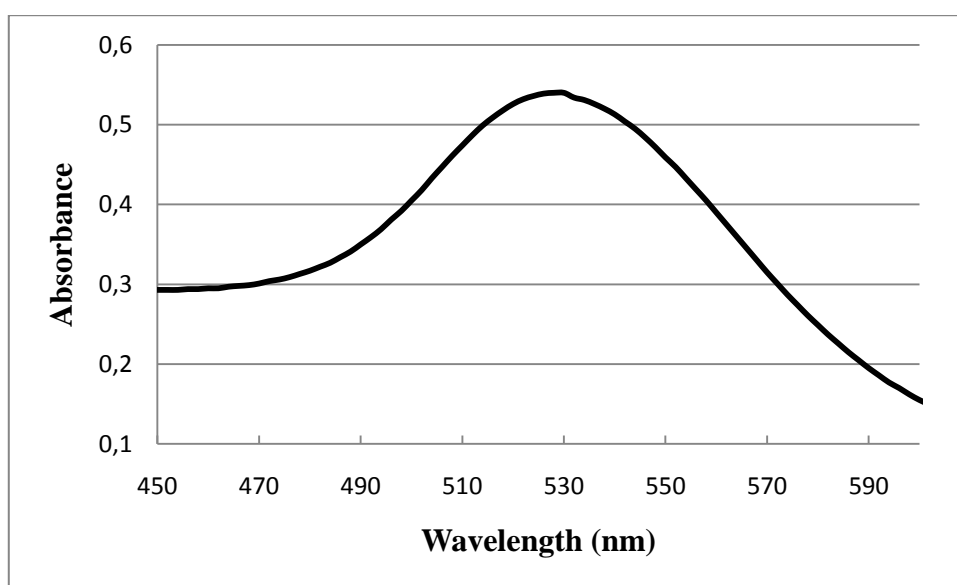


Figure 3.6 Absorption spectrum of gold colloid.

The absorption spectrum (Figure 3.6) showed that maximum absorption of gold colloid was at 530 nm and the peak signal intensity was recorded as 0.536. The data provided by absorption spectrum is in good agreement with the values given in the literature [17].

To confirm morphological character, FE-SEM micrographs of the gold nanoparticles were recorded.

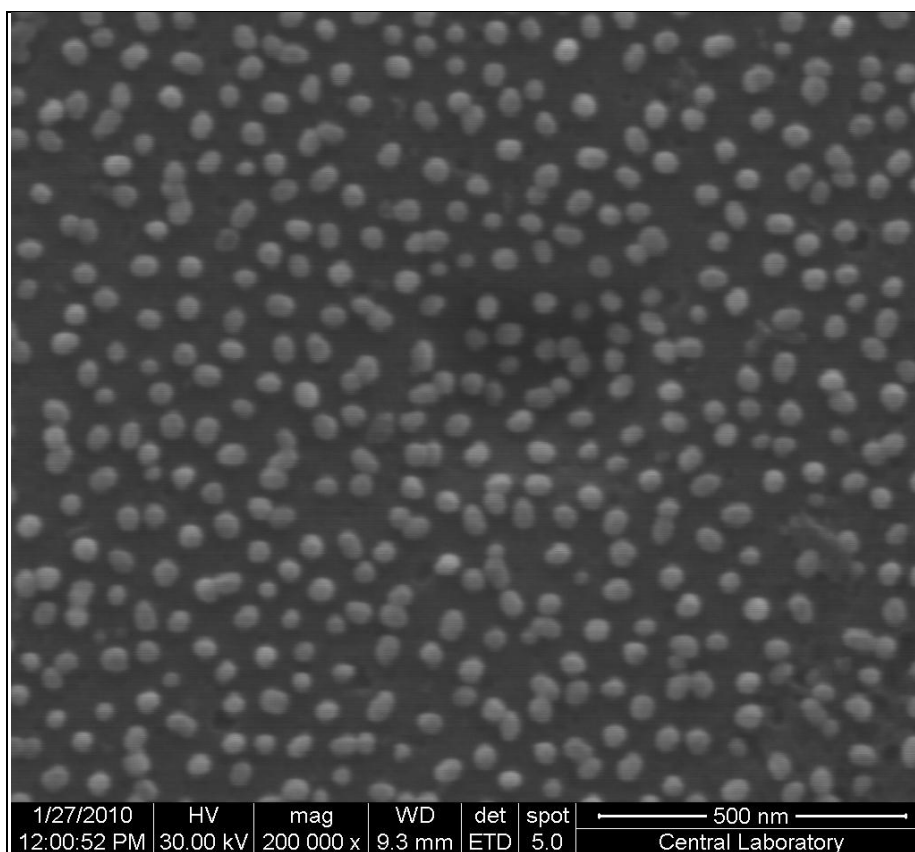


Figure 3.7 FE-SEM image of gold nanoparticles deposited on glass slide.

Obtained FE-SEM image (Figure 3.7) and absorption spectrum exhibited that a monodisperse size distribution with the shape of almost all gold nanoparticles being spherical. The arithmetic average particle diameter was calculated as 37.4 ± 2.3 nm.

While the gold nanoparticles showed more homogenous character in terms of size and shape according to FE-SEM results when compared to silver nanoparticles, silver nanoparticles had stronger absorbance than gold nanoparticles do according to absorption spectra. In other words plasmons of silver nanoparticles were stronger than plasmons of gold nanoparticles.

3.1.3 Silica Coated Silver Nanoparticles

Silica layers with varying thickness were coated on silver nanoparticles in our laboratory. No change in physical appearance in the silver colloid was observed after silica coating.

According to UV-VIS absorption spectra obtained, a red shift was observed. Plasmons of silver colloidal system show maximum absorption at 420 nm (Figure 3.2). However, silica coated silver nanoparticles give maxima at 455 nm. This shift is explained due to the change in refractive index with the presence of silica coating around silver nanoparticles [75].

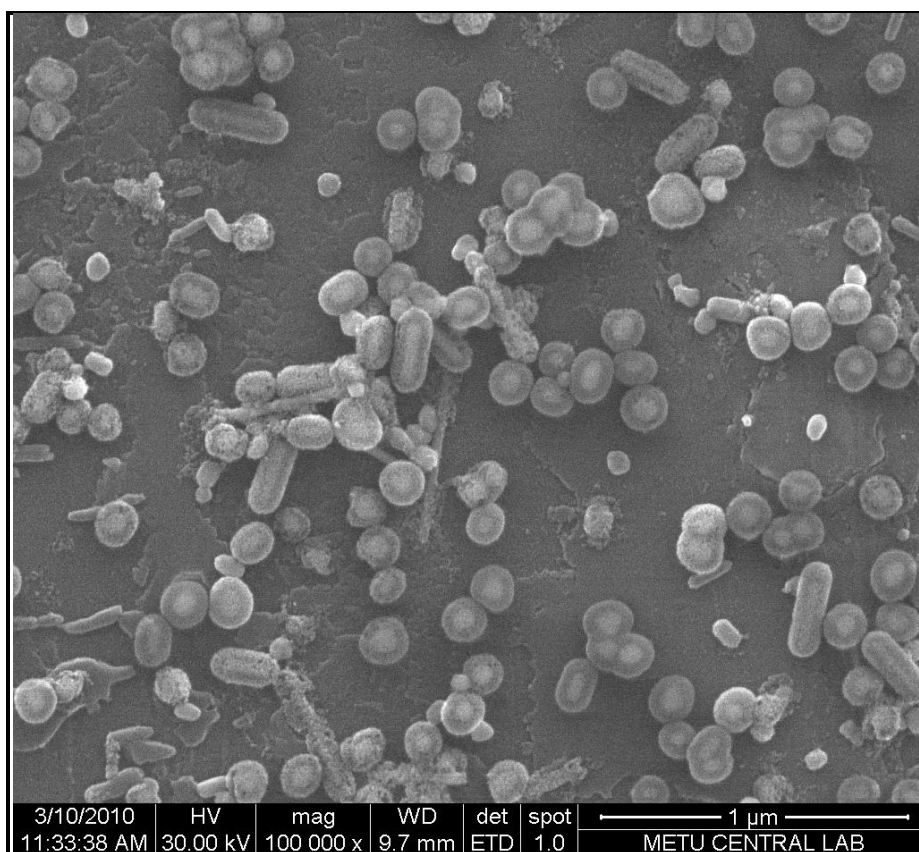


Figure 3.8 FE-SEM image of silica coated silver nanoparticles deposited on glass slide.

In Figure 3.8, the silica coated silver nanoparticles can be seen. The procedure given in section 2.3.1 was used for the preparation of the silver nanoparticles.

Thickness of the coatings showed little variation between particles and was calculated as 43.2 ± 7.3 nm. In Figure 3.8, it could be seen that uniform silica coating was achieved regardless of the shapes of nanoparticles.

3.2 Etching Process

On the assumption that increasing the roughness of the surface or creating small cavities would promote the adsorption of metal nanoparticles on surface, an etching process as described in section 2.5.2 was applied to the glass slides. FE-SEM images of both etched and non-etched substrates were compared (Figure 3.9)

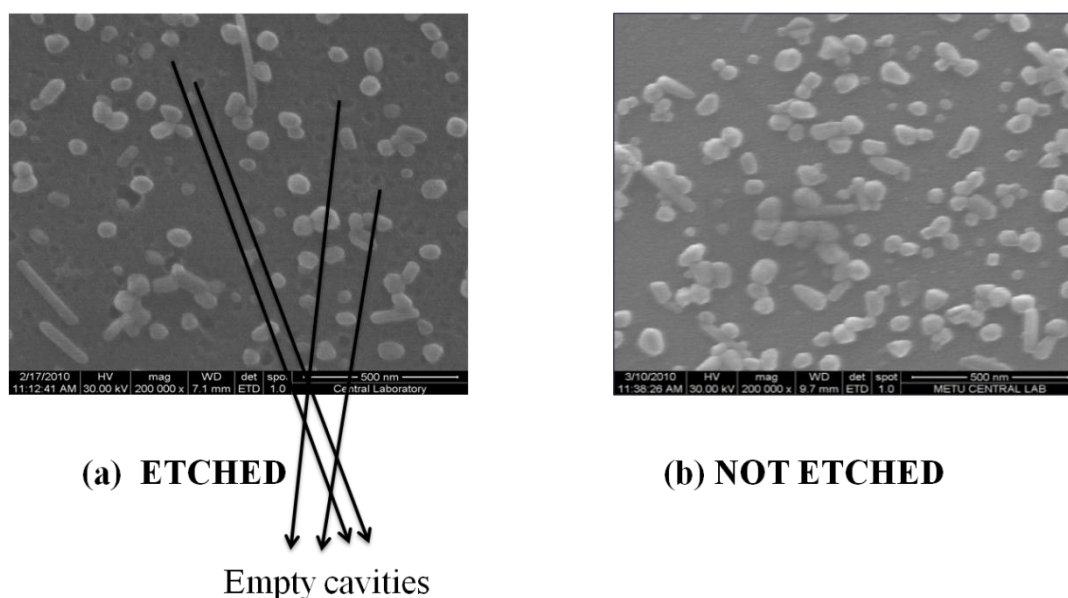


Figure 3.9 FE-SEM images of silver nanoparticles on etched and not-etched glass slides.

FE-SEM images show that nanoparticles did not fill the cavities on etched surface upon deposition (Figure 3.9.a) and etching did not increase the adsorption of nanoparticles on the surface. Therefore, etching was not applied in the following steps of the work.

3.3 Modification (Derivatization) of the Glass Slides Surface

The surfaces of the glass slides were modified as described in section 2.5.3. The clean slides were immersed in 1% (v/v) aqueous APTES solution for 0.5, 1.0, and 3.0 hours.

The procedure given at section 2.6 was applied to modified and unmodified substrates for the deposition of metal nanoparticles. The color difference in the modified and unmodified slides (Figure 3.10) after 24 hours of immersion proven that derivatization was promoting the deposition of metal nanoparticles onto glass surfaces.

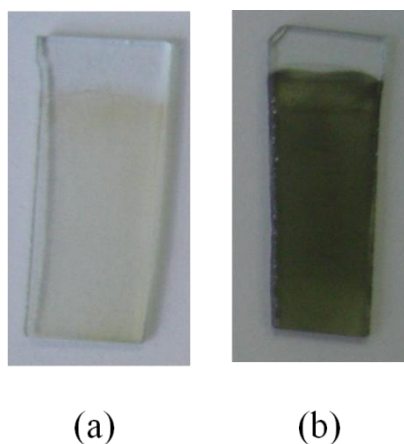


Figure 3.10 Deposition of silver nanoparticles on (a) unmodified and (b) modified surface.

The nature of absorption spectra given in Figure 3.11 is indicative of the fact that silver nanoparticles on modified surface had more intense plasmon absorption than on unmodified slides.

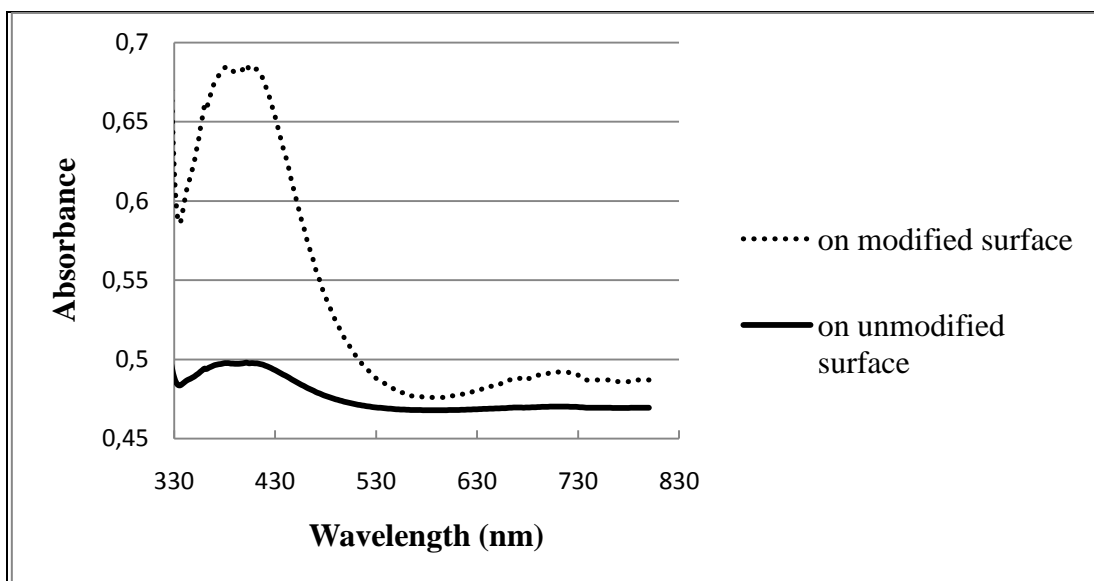


Figure 3.11 Absorption spectra of silver nanoparticles on modified and unmodified surface.

The same effect of derivatization was also observed for gold nanoparticle deposition on glass surface.

Although almost all published research results are in an agreement on the topic of immersion time for derivatization, 0.5, 1.0 and 3.0 hours immersion in APTES were tested and no effect was seen on the deposition quality or quantity of nanoparticles. Therefore 0.5 hour was selected as immersion time for the derivatization procedure.

3.4 Deposition of Nanoparticles on Modified Slides

3.4.1 Immersion Time Optimization – FE-SEM

Deposition of nanoparticles on slides by immersion is a slow but an easy technique when compared to other deposition techniques (e.g. physical vapor deposition). It seems to be slow; however, many slides can be coated at the same time. A disadvantage of the immersion technique is the lower level of homogeneity achieved as compared to some other techniques. Only immersion technique was used for the deposition of metal nanoparticles on the surface.

Immersion time was optimized to find the minimum time of immersion needed for deposition of nanoparticles that resulted in highest surface coverage with maximum plasmon effect.

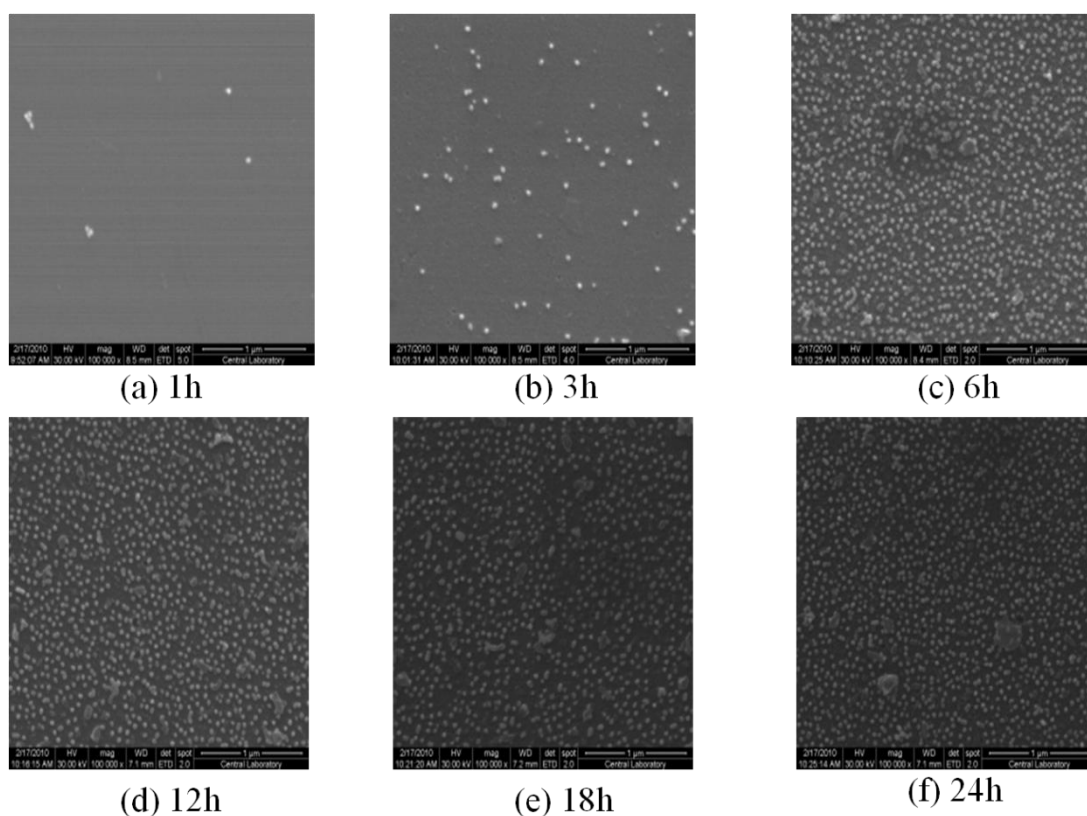


Figure 3.12 FE-SEM images of gold nanoparticles deposited on slides, (a) 1 hour (b) 3 hours (c) 6 hours (d) 12 hours (e) 18 hours (f) 24 hours immersion time.

Gold nanoparticle coated slides with varying immersion times are given in Figure 3.12. It is clearly seen that in the first 3 hours, gold nanoparticles on the surface were few, but when immersion time was increased to 6 hours, surface coverage by gold nanoparticles increased drastically. Immersion time more than 6 hours does not affect the amount of surface coverage (Figure 3.12 d, e, and f). Therefore 6 to 9 hours of immersion was found to be the optimum duration for the desired amount of deposition on the surface.

Same approach to immersion time optimization was taken for silver nanoparticles (Figure 3.13).

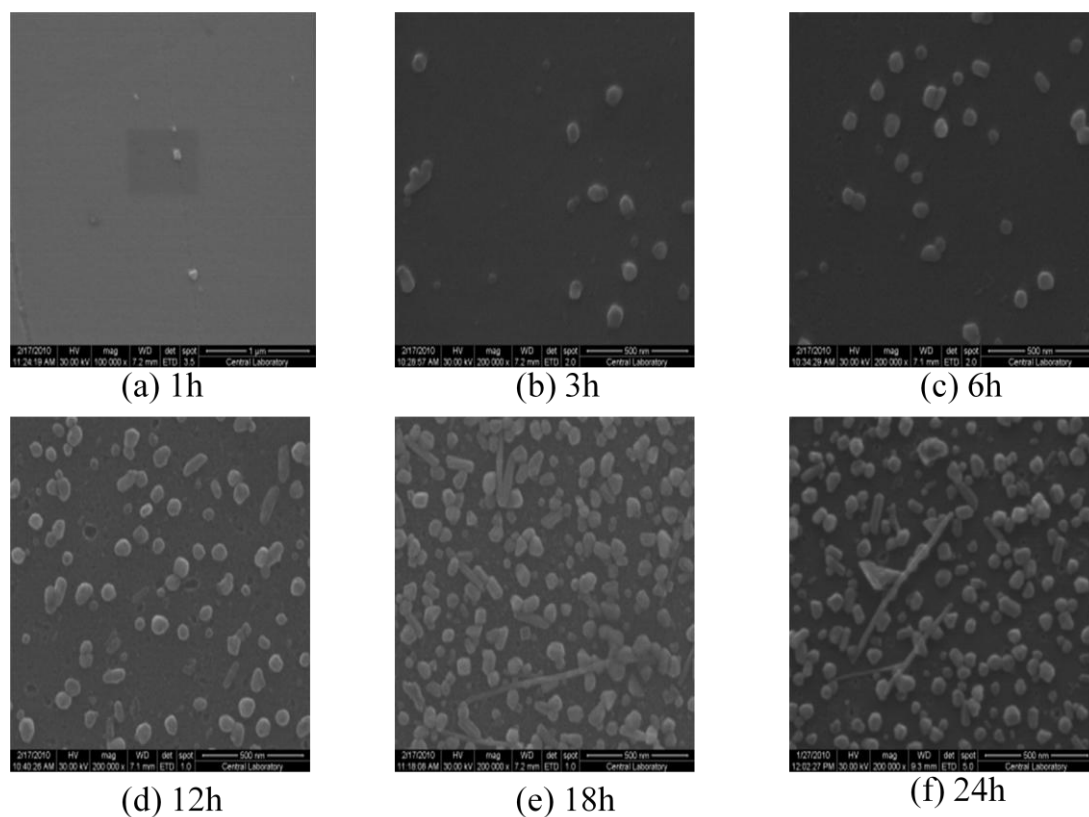


Figure 3.13 FE-SEM images of silver nanoparticles deposited on slides, (a) 1 hour (b) 3 hours (c) 6 hours (d) 12 hours (e) 18 hours (f) 24 hours immersion time.

According to the FE-SEM images in Figure 3.13, 18 hours of immersion time was optimal for high surface coverage as after 18 hours surface coverage was not improving.

3.4.2 Absorption Spectra of Metal Nanoparticle Coated Slides

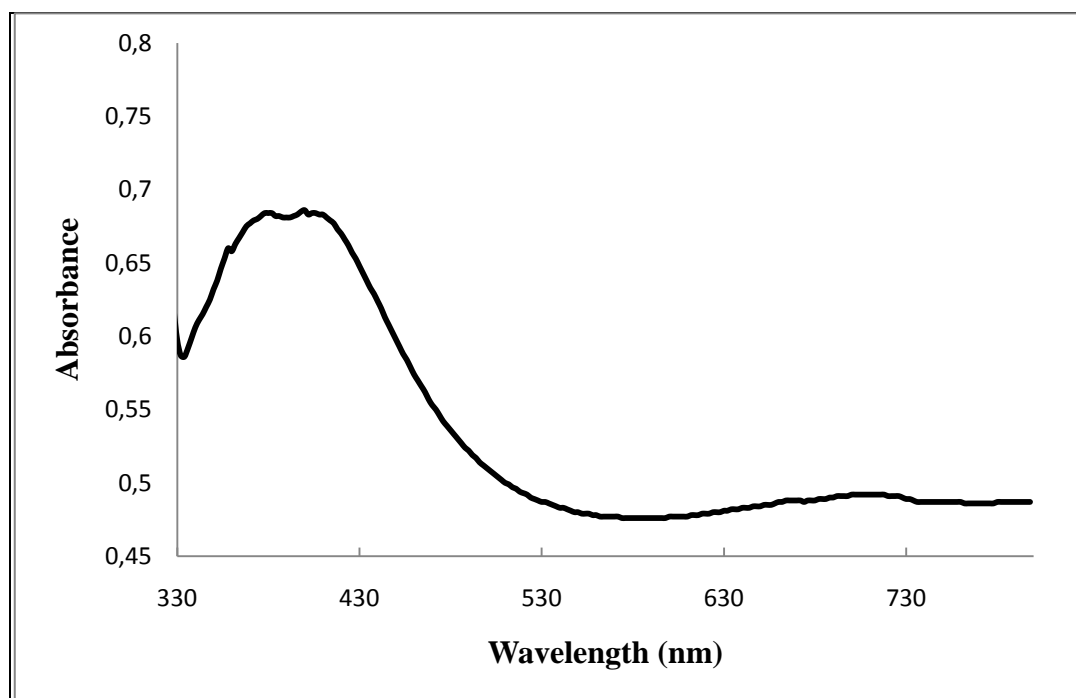


Figure 3.14 Absorption spectrum of silver nanoparticles coated glass slide (18 hours of immersion).

When Figure 3.14 was compared with figure 3.2, it was observed that the signal intensity was lower and the peak was broader in Figure 3.14 than in Figure 3.2. Firstly, the signal of nanoparticles deposited on the surface was lower because of the path length. For silver colloid absorption spectrum (Figure 3. 2), a standard UV-VIS cell with 1 cm path length was used. On the other hand, for the spectrum of nanoparticles on substrate, the path length was only the radius of nanoparticles itself (<100nm) if monolayer formation of metal nanoparticles could be assumed according to FE-SEM images recorded. The maximum absorption peak was again at around 400-430 nm but broader due to aggregation of some silver nanoparticles on the surface. The broad plasmon band with the peak at around 700 nm could be attributed to the presence of non-spherical, rod shaped nanoparticles deposited [76].

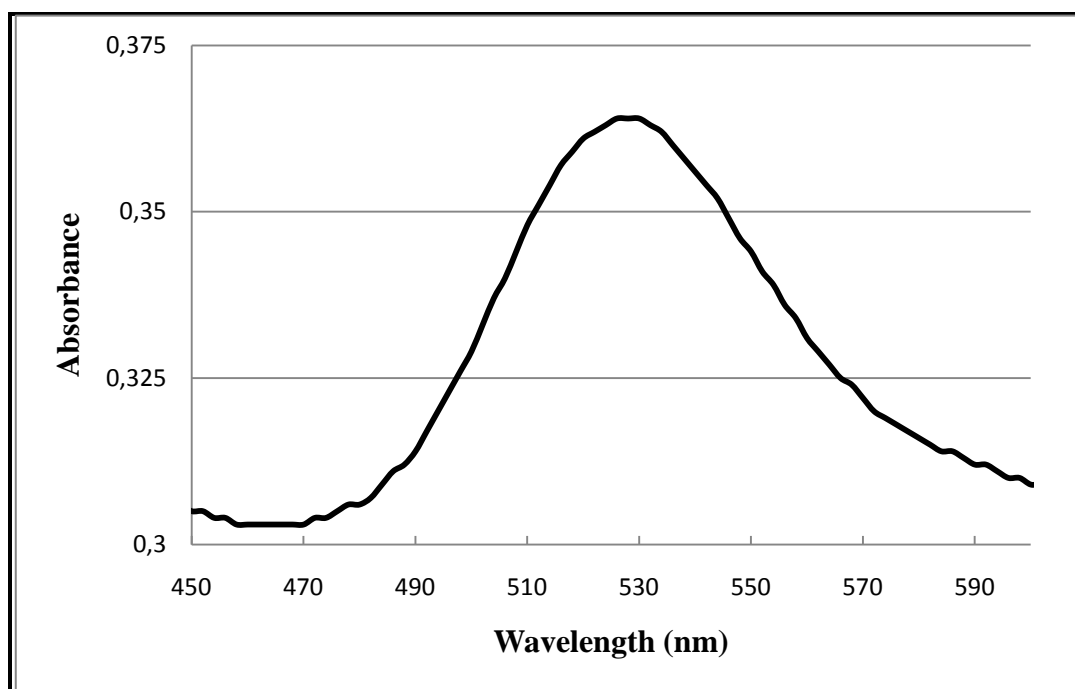


Figure 3.15 Absorption spectrum of gold nanoparticles coated glass slide (9 hours of immersion)

Gold nanoparticles deposited on glass surface had the maximum absorption peak at 530 nm as with gold colloid (Figure 3.5). However, there was no broadening of the absorption peak for deposited gold nanoparticles when it was compared with gold colloid system (Figure 3.5).

According to FE-SEM images recorded, gold nanoparticles seemed to be adsorbed homogeneously whereas, silver nanoparticles showed aggregation on the modified glass slides.

3.5 Use of Metal Nanoparticle Coated Surface as a Surface Enhanced Raman Scattering (SERS) Substrate

Effect of nanoparticles on the Raman signal intensity of Brilliant Cresyl Blue (BCB) solution is given in Figure 3.16.

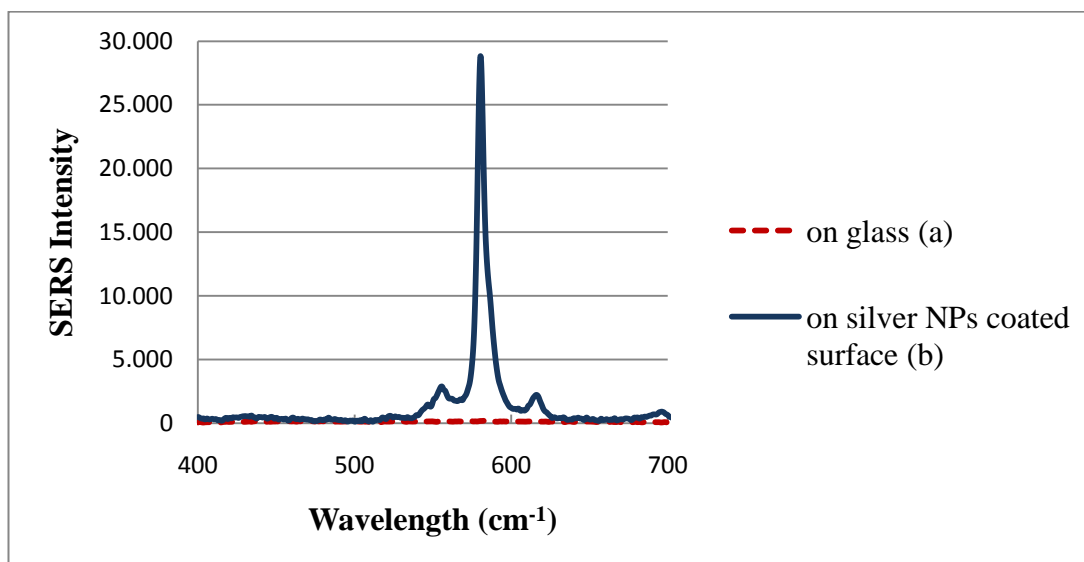


Figure 3.16 Effect of silver nanoparticles coated surface on SERS intensities of 1.0×10^{-6} M Brilliant Cresyl Blue (BCB) drop, (a) on glass, (b) on silver nanoparticles (NP) coated glass surface

The signal at 580 cm^{-1} is due to the benzene ring in Brilliant Cresyl Blue (BCB). Raman spectrum taken with 1.0×10^{-6} M aqueous solution of BCB didn't yield any signal discernible from background. Increasing the concentration 1000-fold resulted in a characteristic peak at 580 cm^{-1} . It could be clearly seen that, the SERS signal intensity was increased due to the electromagnetic field of surface plasmons (SPs).

3.5.1 Immersion Time Optimization - SERS

Effect of immersion time has been investigated by comparing the recorded FE-SEM images in section 3.5.1. However, it is also important to compare the SERS signal enhancement of prepared substrates to assign the optimum immersion time, as the Raman spectrum gives an idea about the enhancement field of the surface plasmons. A $10 \text{ }\mu\text{l}$ drop of 1.0×10^{-6} M of BCB solution was placed on silver nanoparticles coated and bare glass slides prepared with varying immersion times during the deposition step.

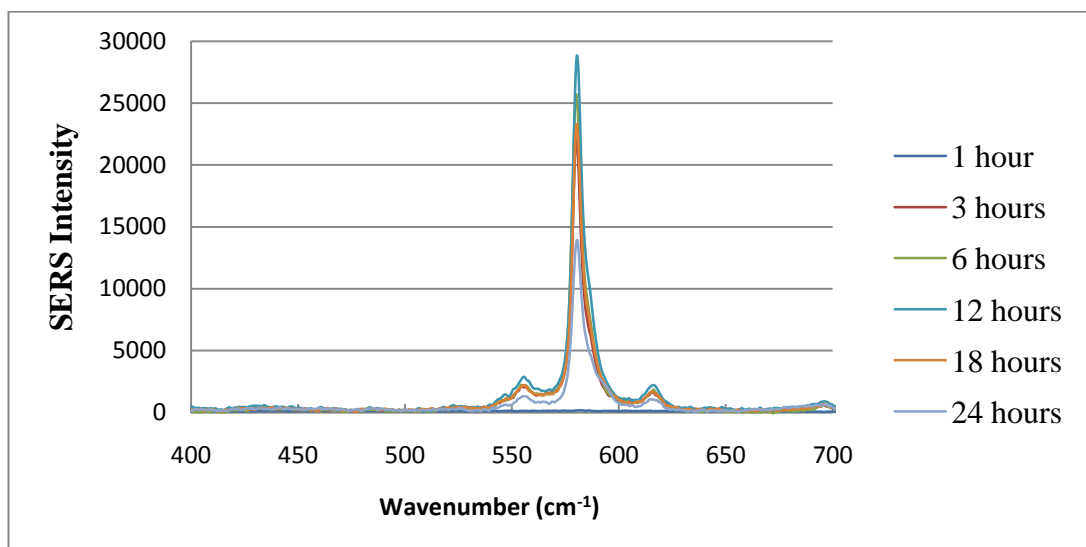


Figure 3.17 Effect of nanoparticle deposition immersion time on the SERS signal enhancing of silver nanoparticles coated substrates on BCB

The effect of nanoparticle deposition immersion time on the SERS spectra of BCB is given in Figure 3.17

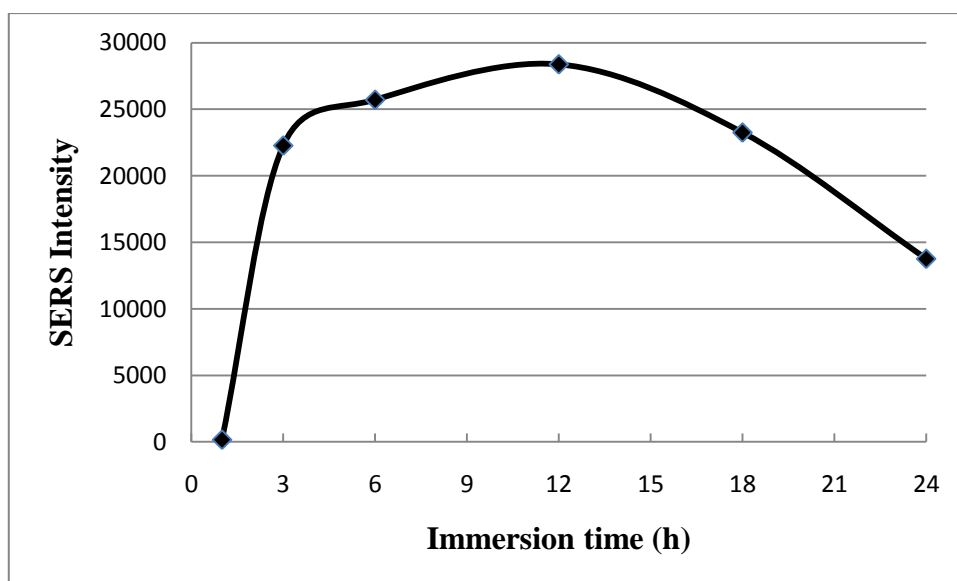


Figure 3.18 SERS intensity of 10^{-6} M BCB solution versus immersion time (h).

As discussed in section 3.5.1, 18 hours of immersion was minimum for the deposition of nanoparticles on the surface with maximum surface coverage according to recorded FE-SEM images. In Figure 3.13 it is shown that, only a few numbers of silver nanoparticles were on the surface when substrate was immersed for only one hour. Hence, no effect on the Raman signal of 10^{-6} M BCB solution was

observed with this substrate. The enhancement was increasing linearly as the immersion time increases up until the immersion time was 12 hours (Figure 3.18). The SERS effect of nanoparticles deposited with 18 and 24 hours of immersion time was lower than 12 hours of immersion. At this point, FE-SEM images can be used as a proof of aggregation of nanoparticles after 18 hours of immersion in colloidal system. If the APTES-modified glass slide was kept in colloid for more than 12 hours, the surface got very crowded and the probability of aggregation was higher. As a result of FE-SEM images (2.6.1) and SERS spectra of 10^{-6} M BCB (Figure 3.17), 12 hours was set as the optimum time for immersion and the surface enhanced fluorescence SEF substrates were prepared accordingly.

3.5.2 Stability of Silver Nanoparticle Coated Substrates

Since gold nanoparticles are known to be more stable than silver nanoparticles, only silver nanoparticle coated substrates were tested for stability as explained below. A 10 μ l drop of 10^{-6} M Brilliant Cresyl Blue (BCB) solution was placed on the silver nanoparticle coated substrate and the surface enhanced Raman scattering (SERS) spectrum was measured. The measurement was repeated with the same substrate 15 days later. Both SERS spectra are shown in Figure 3.19. During the two weeks, the substrates were kept in dessicator at dark.

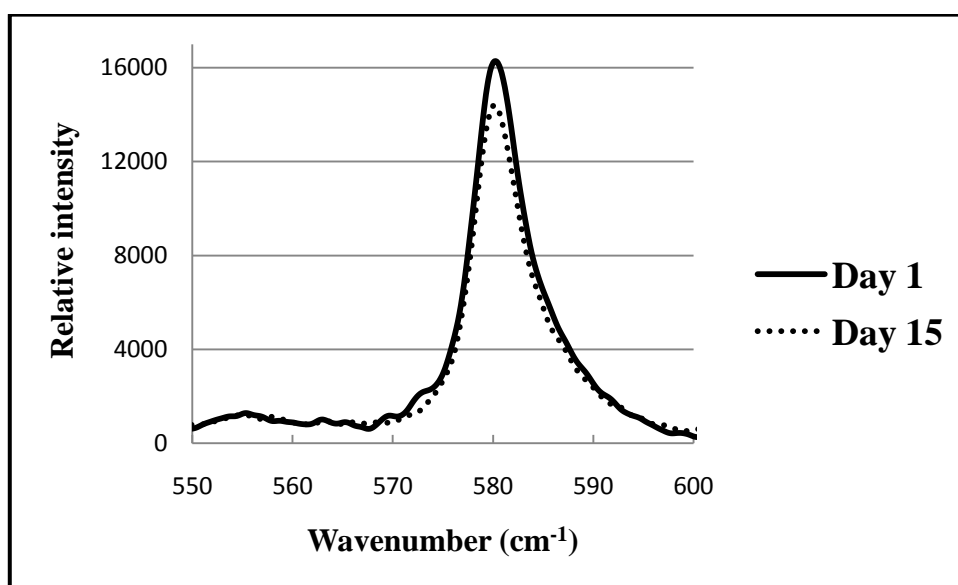


Figure 3.19 SERS spectra of BCB on freshly prepared silver nanoparticle coated substrate and two weeks later.

In Figure 3.19, it is shown that, the enhancement due to the presence of silver nanoparticles was slightly diminished. However, it should be noted that the enhancement factors for fresh and aged substrate were still in the same order of magnitude, therefore it can be said that the substrate preserved its plasmonic properties for the duration of two weeks under the conditions of storage.

3.6 Preparation and Evaluation of Surface Enhanced Fluorescence (SEF) Substrates

Spacer layers of various types of material and thickness were formed on the prepared nanoparticle deposited glass slides. The fluorescence enhancement effect of the resulting SEF substrates were examined using rhodamine B and fluorescein as fluorophores. The SEF substrates given in Table 3.1 were prepared.

3.6.1 Silica and Zinc oxide Layers on Silver Nanoparticle Coated Substrates

Silica layers were deposited on silver nanoparticle coated glass slides by sputtering technique as described in section 2.2.6. The sputtering system was calibrated for thickness control of deposited layers by researchers in Physics Department, METU prior to the deposition. Changes in optical absorption spectra due to varying silica spacer layer thickness were observed (Figure 3.20).

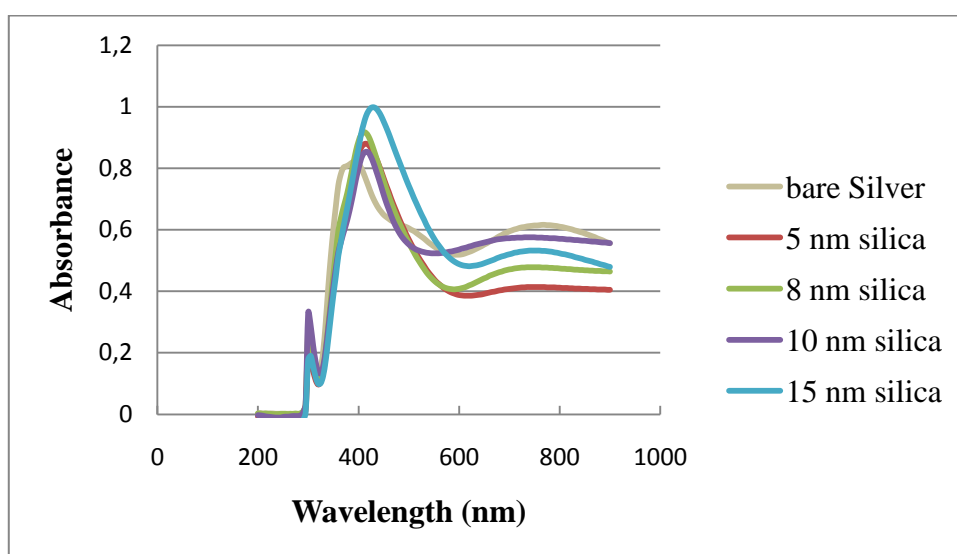


Figure 3.20 Absorption spectra of silver nanoparticles coated substrates with different thickness of silica layers.

As seen in Figure 3.20, a red shift was observed from the spectrum of substrate with only silver nanoparticles when 5 nm of silica layer was present on the substrates. It was not observed any significant change when thickness was increased from 5 nm to 10 nm. However, 15 nm thickness of silica showed a distinctive red shift. The observed overall red shift attributed to the refractive index change when silica layer was deposited on silver island films. This was almost the same result as compared with the spectra of silver nanoparticles coated with silica in colloidal phase explained in section 2.3.3.

Absorption spectrum of zinc oxide spacer layer formed with sputtering technique was presented below (Figure 3.21).

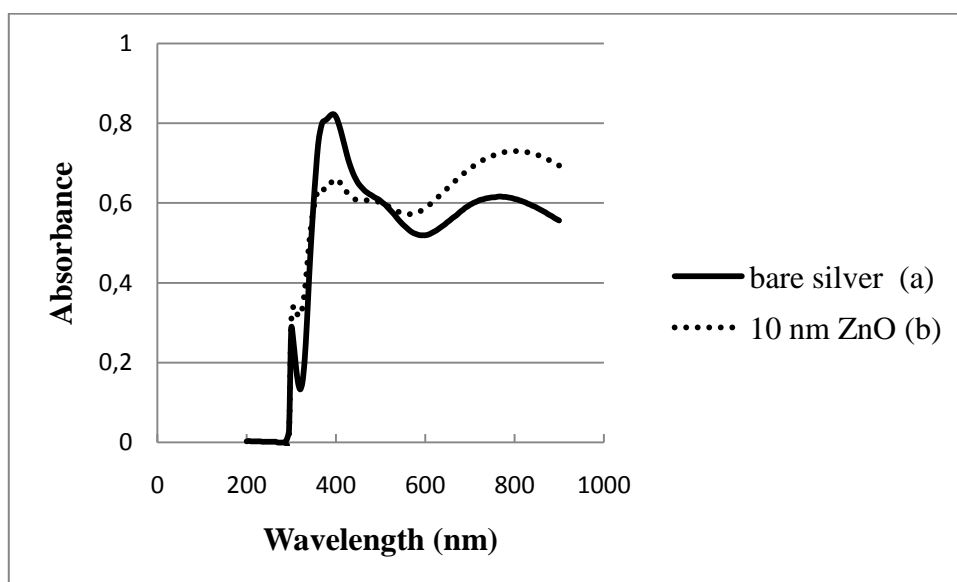


Figure 3.21 Absorption spectra of (a) silver nanoparticles coated substrate (b) 10 nm ZnO coated on silver nanoparticles coated substrate.

The absorption spectra of silver nanoparticles on glass slide with zinc oxide spacer layer showed that the intensity of absorption peak at 400 nm, attributed to spherical silver nanoparticles decreased. Also, the intensity of the absorption band at 600-800 increased.

3.6.2 Gold Layer on Silver Nanoparticle Coated Substrates

Absorption spectrum of 10 nm gold spacer layer formed with thermal evaporation technique was presented below (Figure 3.22).

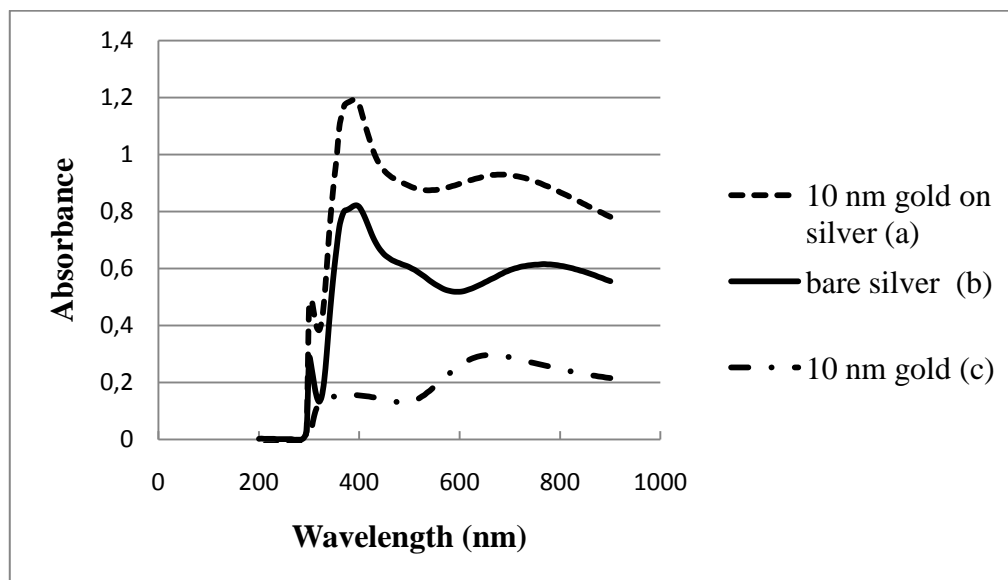


Figure 3.22 Absorption spectra of (a) 10 nm gold deposited silver nanoparticles coated substrates, (b) only silver nanoparticles coated substrate, (c) only 10 nm gold deposited substrate.

As can be seen in Figure 3.22, 10 nm gold layer deposited on glass slide exhibited an absorption band at 600-800 nm. The plasmon absorption spectra of gold layer on silver nanoparticles combined constructively (Figure 3.22).

3.6.3 Formation of Stearic Acid Molecular Layers on Silver Nanoparticles Coated Substrates

In this part, spacer layers of stearic acid deposited by Langmuir-Blodgett (LB) film system was evaluated and it was investigated whether monomolecular LB deposition can be an alternative method to physical vapor deposition (PVD) techniques for deposition of spacer layers.

As with the inorganic spacer layers deposited by PVD explained in previous sections, the distance dependency of SEF to the metal surface was studied by

changing the number of stearic acid layers between silver nanoparticles and fluorophores.

3.6.3.1 Isotherm Experiments and Target Surface Pressure

The isotherm experiment was performed as described in 2.7.3 in order to find the optimum surface pressure for LB deposition for 20 μl of 1.0 mg/ml stearic acid solution in chloroform spread on aqueous subphase.

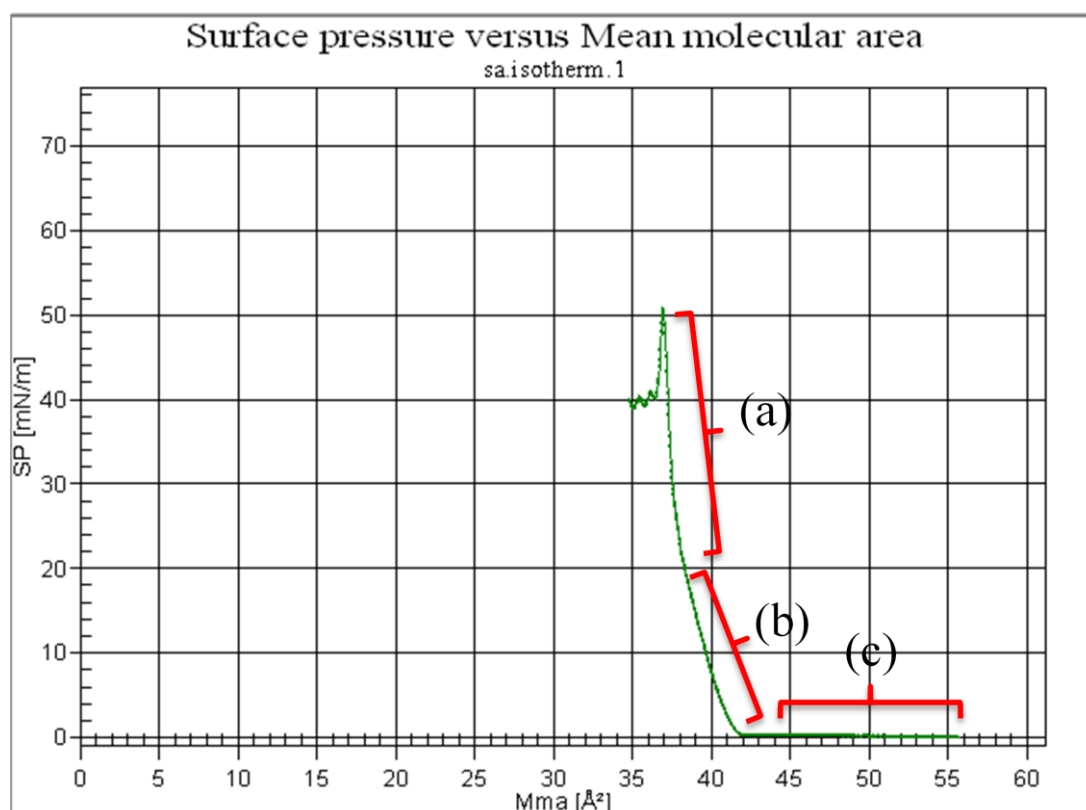


Figure 3.23 Surface pressure – Mean molecular area per stearic acid molecule (π -A) isotherm of stearic acid monolayer (green line), region (a) solid, (b) liquid (c) gas phase.

As can be seen in Figure 3.23, where surface pressure is plotted against mean molecular area per stearic acid molecule, surface pressure was almost zero until 42 \AA^2 mean molecular area per stearic acid molecule, which indicated stearic acid monolayer was in “gaseous” phase in this region. The surface pressure started to increase between 37-42 \AA^2 (“liquid” phase) and a sharper increase was observed when mean molecular area per stearic acid dropped below 38 \AA^2 ; stearic acid

molecules were arranged as “solid” phase in the range of 37 to 38 Å². While compression continued, surface pressure suddenly dropped at a certain point where the monomolecular layer collapsed and micelles were formed.

As conclusion of the isotherm experiment, the so-called “phase transition behavior” of the stearic acid monolayer spread on aqueous subphase was determined and the surface pressure was measured to be between 23 and 50 mN/m where the monolayer can be defined as in “solid” phase. While the orientation of the monolayer at the highest surface pressure (~50 mN/m) may be preferred for deposition, it is not possible to keep the surface pressure exactly at this instable point during dipping and the monolayer can easily collapse. So, 30 mN/m was chosen as target surface pressure for deposition. Obtained target surface pressure was in agreement with literature values.

3.6.3.2 Dipping Experiments

The dipping was performed as described in section 2.7.3. Y-Type deposition was applied to the substrates.

Up to 5 layers of stearic acid (SA) have been formed on silver nanoparticle coated substrates. Expected structures are given in Figure 3.24.

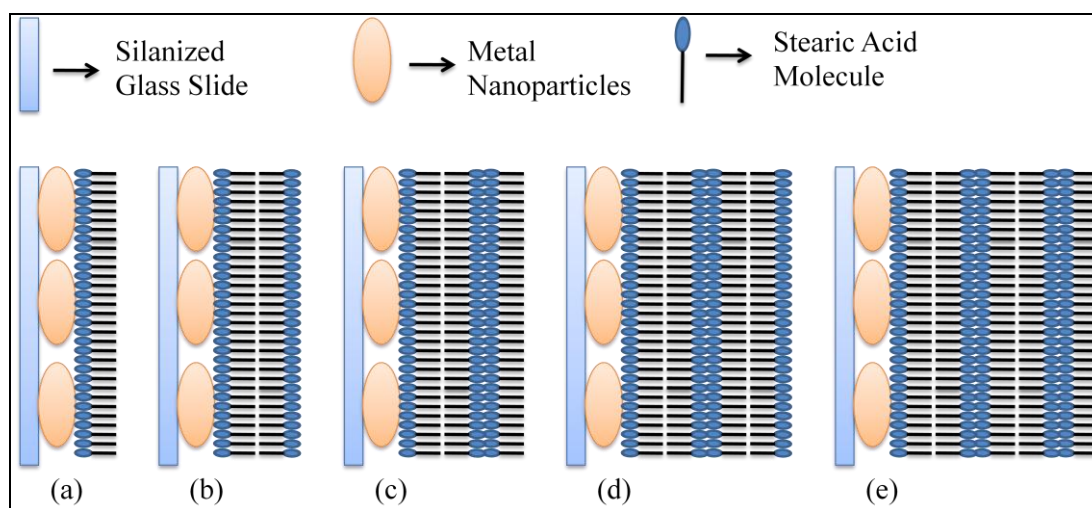


Figure 3.24 Y-type LB deposition of stearic acid layers, (a) 1 layer, (b) 2 layers, (c) 3 layers, (d) 4 layers (e) 5 layers.

Silver nanoparticles coated substrates display hydrophilic character [77]. After the formation of the first stearic acid layer (Figure 3.24.a) the surface became

hydrophobic. This change in surface character confirmed formation of stearic acid layer. The deposited region of the substrate was also different in appearance than the rest of the substrate.

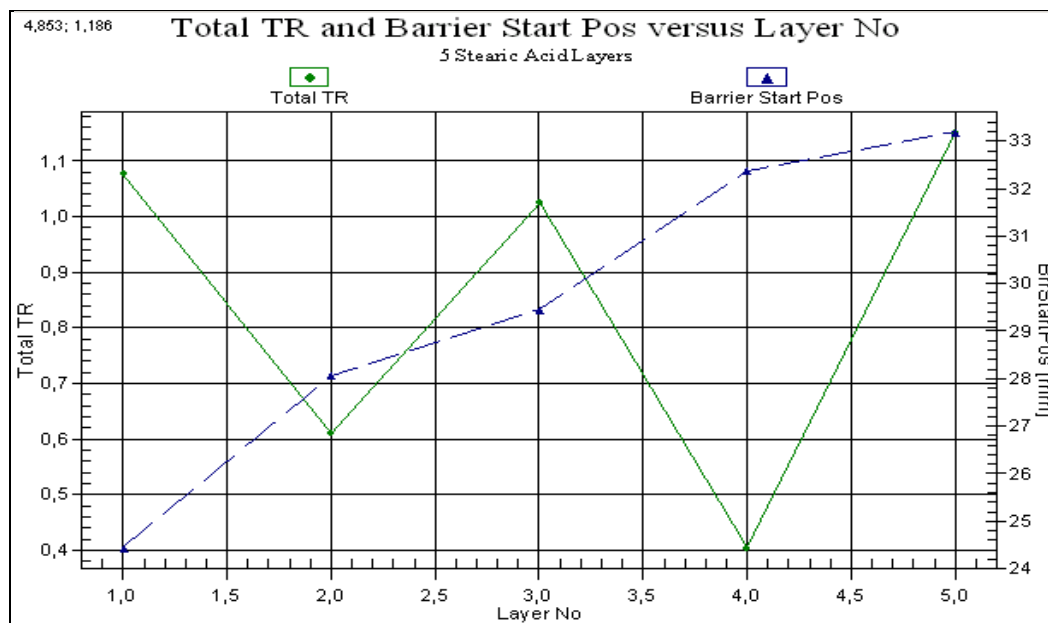


Figure 3.25 Graph of transfer ratio, barrier, position versus layer no.

Transfer ratio for each layer was calculated in real time by the LB control software. Transfer ratio (TR) is the ratio of the decrease in monolayer area during deposition (A_1) to the area of substrate deposited (A_2). Area A_1 equals to the sum of areas (A) represented in Figure 3.26.

The movement of the dipper arm that holds substrates and the barriers were controlled by sensitive stepper motors. Movements of both dipper and barriers were accurately monitored in real time and precisely controlled by the software. The software calculated area A_1 and A_2 from positional changes of barriers and dippers, respectively. If the area of the substrate is entered correctly, the transfer ratio calculated by the software is further proof of the desired formation of layers. Figure 3.25 showed the changes in barrier position between 24 and 33 mm (blue dashed line) while the target pressure was maintained and the green line represents the total transfer ratio (TR) in each layer formation.

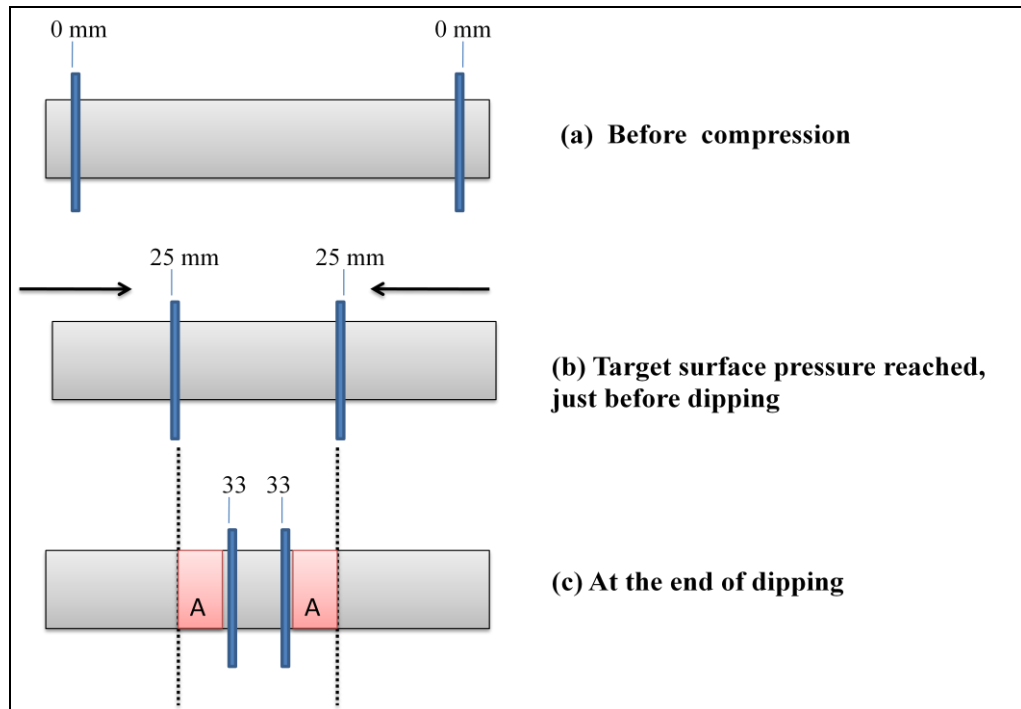


Figure 3.26 Position of barriers (a) zero position, (b) at target surface pressure, (c) at the end of dipping experiment.

Table 3.3 TR values obtained after 5 layers of stearic acid deposited.

Layer No	Direction	Total TR	Upper Limit (mm)	Lower Limit (mm)
1	Up	1.076	3.00	-20,01
2	Down	0.610	3 00	-20,01
3	Up	1.025	3.00	-20,01
4	Down	0.404	3.00	-20,01
5	Up	1.152	3.00	-20,01

As can be seen in Table 3.3, the transfer ratios during upstroke deposition were close to unity (Layer No 1, 3, and 5). Thus, it can be inferred that transfer of monolayer to the substrate was established. However, the TR values were not close to unity during downstroke dipping.

3.7 Surface Enhanced Fluorescence (SEF) Studies

Rhodamine B and fluorescein were chosen as fluorescent dyes. Excitation and emission wavelength of fluorescent dyes were determined (Section 3.8.1). In order to enhance the emission signal intensity of fluorescent dyes, both colloid mixture of metal nanoparticles and prepared SEF substrates with different spacers were used. For solution based fluorescence enhancement; varying amount of silver, gold and silica coated silver colloid mixtures were mixed with aqueous solution of rhodamine B and fluorescein. For surface studies, prepared SEF substrates were used as described in section 2.1.

3.7.1. Fluorescence Properties of Rhodamine B and Fluorescein

Rhodamine B and fluorescein were chosen for SEF experiments in this work. Their solutions were prepared according to the procedure described in Section 2.4. The excitation and emission spectra belonging to these solutions are presented below.

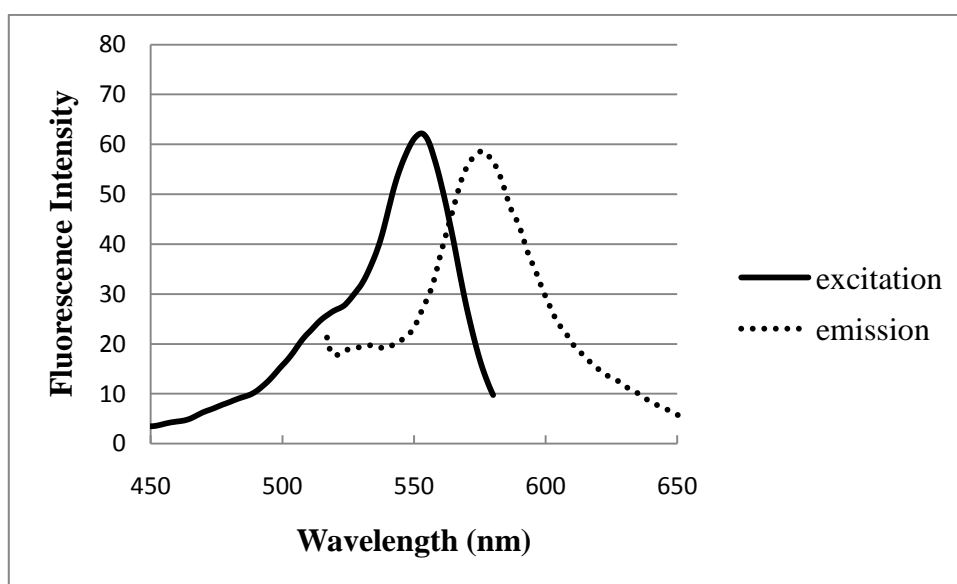


Figure 3.27 Excitation and emission spectra of rhodamine B.

As seen in Figure 3.27, excitation and emission wavelengths of rhodamine B were found to be 490 and 579 nm, respectively.

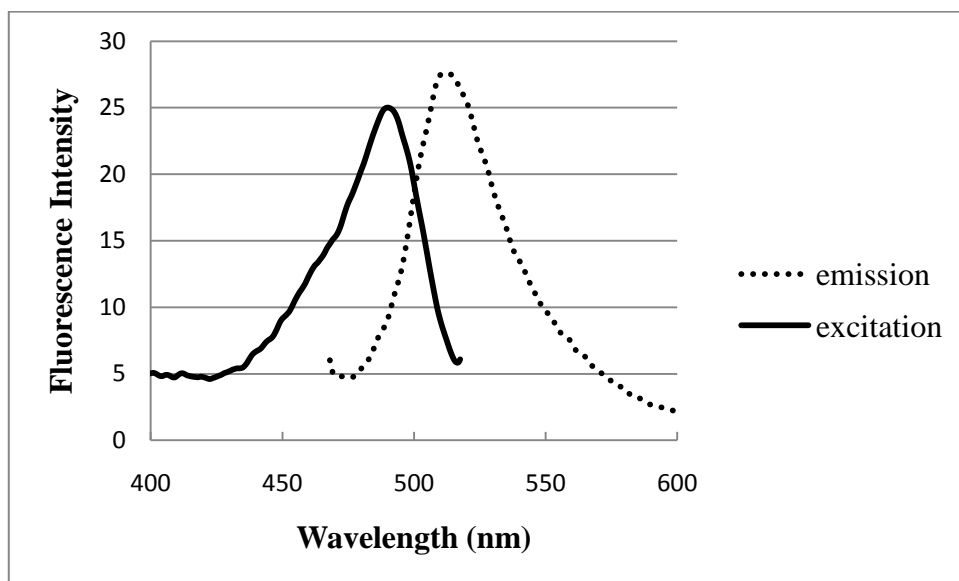


Figure 3.28 Excitation and emission spectra of fluorescein.

Excitation and emission wavelengths of fluorescein were found to be 490 and 513 nm, respectively.

3.7.2 SEF in Solution

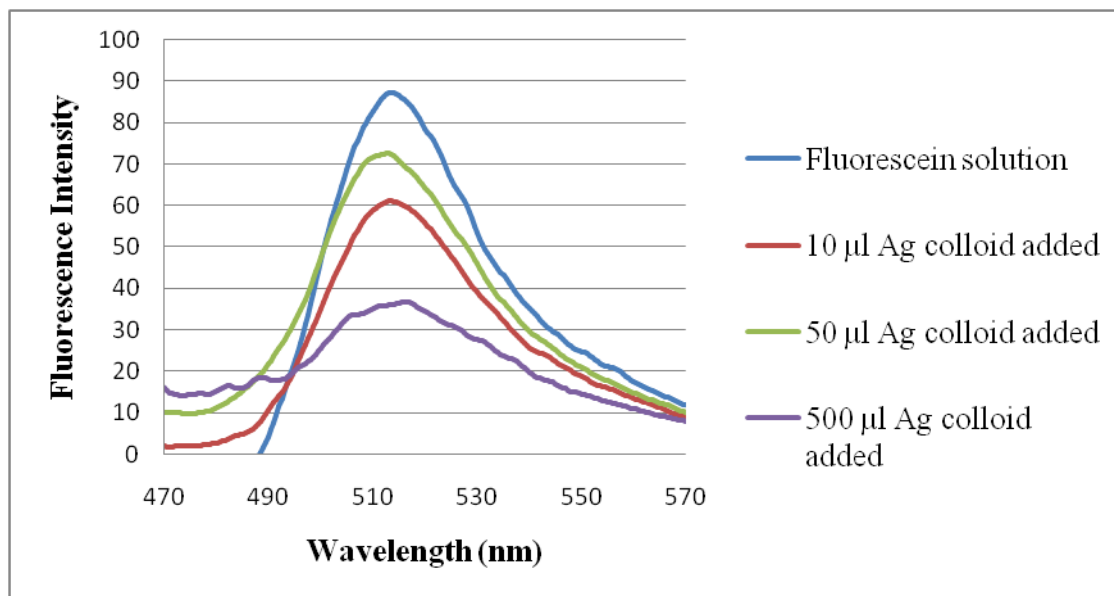


Figure 3.29 Effect of silver colloid to the fluorescence of 10^{-7} M fluorescein solution.

The concentration of fluorescein was kept 10^{-7} M for all experiments and different amounts of silver colloid (prepared as described in section 2.3.1) were added. According to Figure 3.29, first the fluorescence signal intensity was quenched by addition of silver colloid. This quenching attributed to the possible energy transfer from fluorescein molecules to silver nanoparticles.

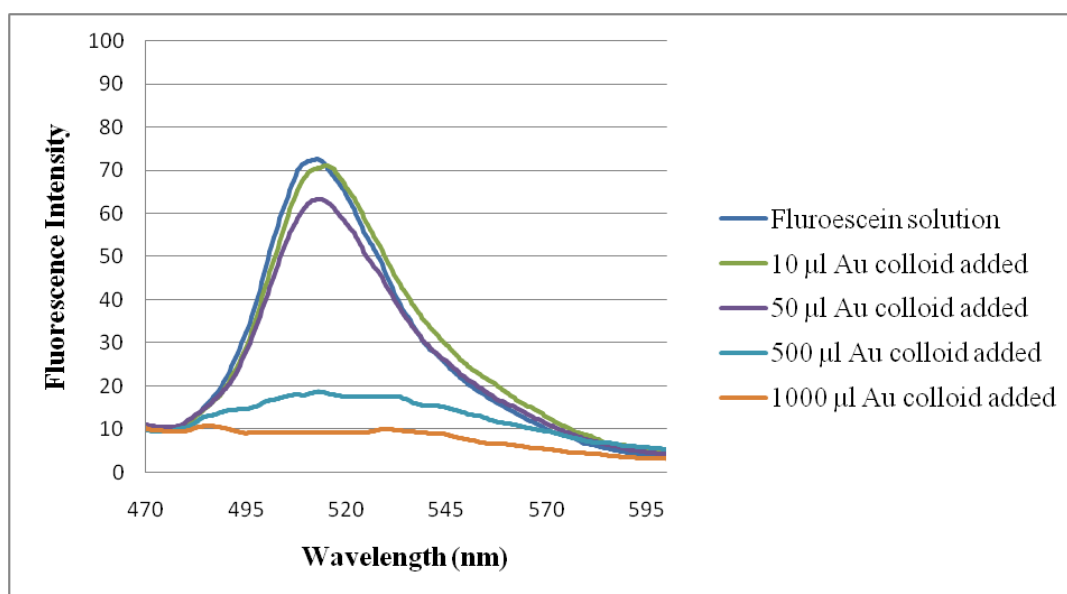


Figure 3.30 Effect of gold colloid to the fluorescence of 10^{-7} M fluorescein solution.

In Figure 3.30, it is shown that addition of gold colloid decreased the emission intensity of fluorescein solution. However, when 500 and 1000 μl gold colloid were added, the fluorescence signal was quenched very sharply when compared to the effect of silver colloid.

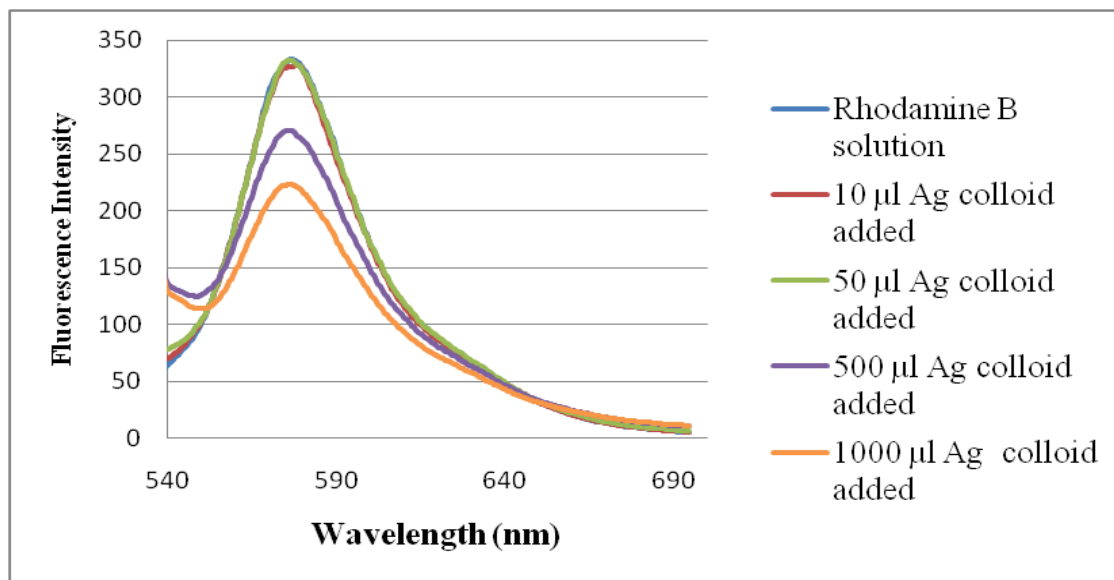


Figure 3.31 Effect of silver colloid to the fluorescence of 10^{-6} M rhodamine B solution.

Little amount of (10 and 50 μl) silver colloid addition to the 10^{-6} M rhodamine B solution almost did not affect the fluorescence signal intensity of Rhodamine B (Figure 3.31, overlapping peaks). When the amount of silver colloid addition was increased to 500 and 1000 μl , the rhodamine B emission intensity was affected negatively and the emission was quenched. The quenching was not as strong as in the case of fluorescein-gold interaction.

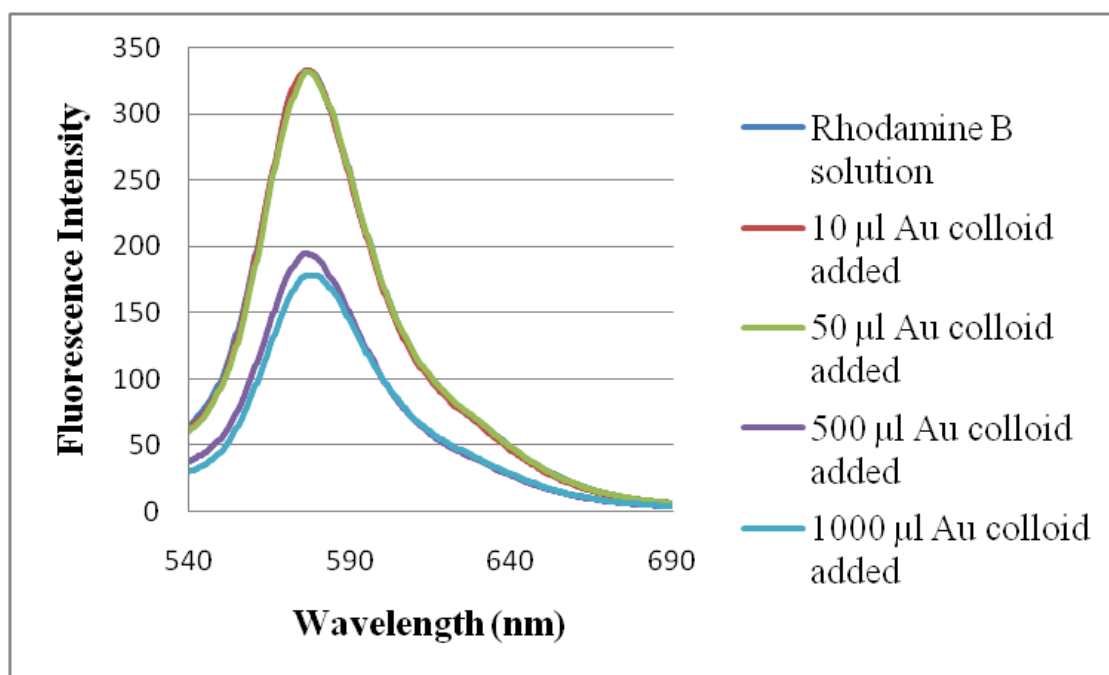


Figure 3.32 Effect of gold colloid to the fluorescence of 10^{-6} M rhodamine B solution.

As silver colloid, gold colloid inhibits the emission signal of Rhodamine B solution when amount of colloid increased. In Figure 3.32, it is seen that 1000 µl and 500 µl gold colloid additions quenched the emission of rhodamine B intensity due to the Förster resonance energy transfer between rhodamine B molecules and gold nanoparticles.

Silica coated silver nanoparticles were prepared as described in section 2.3.3. The silica coating around silver nanoparticles was applied in order to create a barrier between fluorophore and silver nanoparticles to avoid energy transfer. The effect of silica coated silver nanoparticles to the emission intensity of rhodamine B solution is given in Figure 3.33 below.

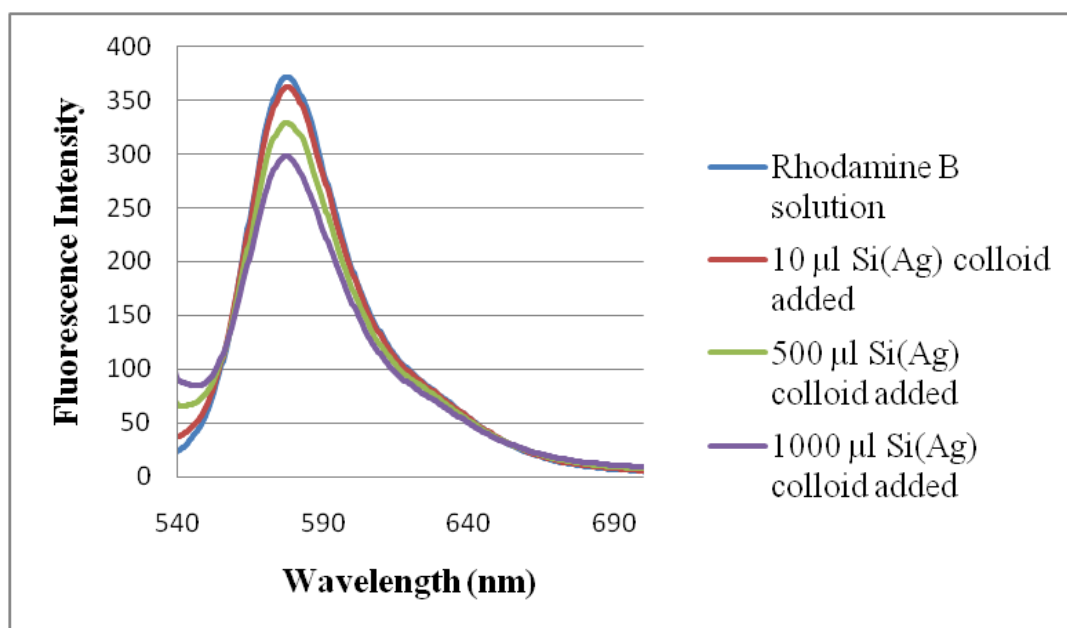


Figure 3.33 Effect of silica coated silver colloid to the fluorescence of 10^{-6} M rhodamine B solution.

Silica coated silver colloid was mixed with Rhodamine B solution with varying proportions, while Rhodamine B concentration were kept constant (10^{-6} M). According to results in Figure 3.33, addition of silica coated silver colloid did not affect as strong as bare silver colloid did. The decrease in the quenching effect of silver colloid could be assigned to the silica coating. The silica coating was thick enough to stop quenching but not thin enough to provide the optimal distance for enhancement. In other words, metal nanoparticles were far from rhodamine B molecules for energy transfer. Also, rhodamine B molecules are far from electromagnetic field of surface plasmons.

3.7.3 SEF on Surface

Incident light angle was optimized by use of homemade rotatable stand described in section 2.2.1. 10 μl 1.0×10^{-4} M of rhodamine B solution was dropped on the glass slide (section 2.5). Afterwards, another glass slide was placed on it. Two sides of the glass slides were squeezed with a paper clamp tool. By this way, rhodamine B solution was spread through entire surface and kept between the slides. A very short path length was provided. This sandwich like sample cell was placed on the homemade stand vertically.

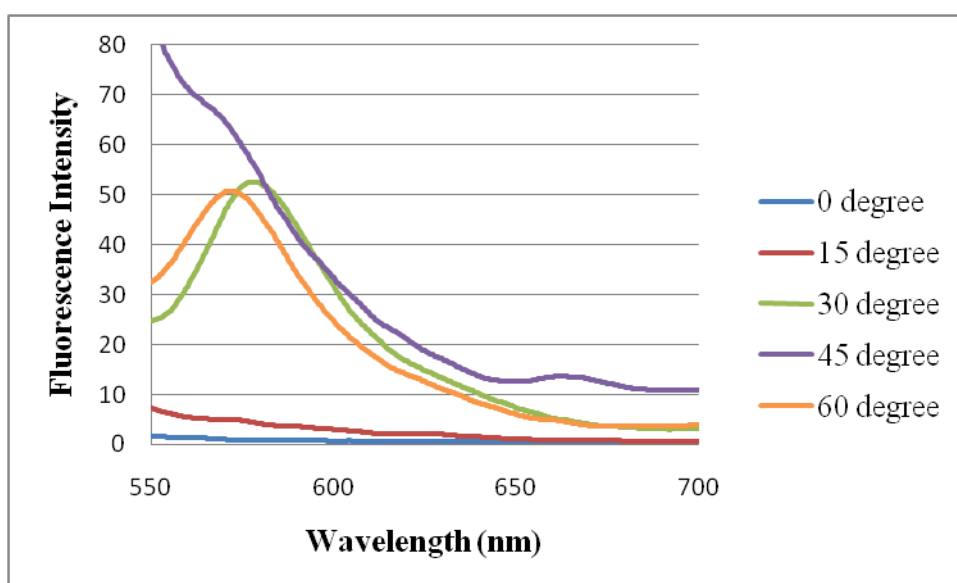


Figure 3.34 Incident light angle optimization for SEF measurements.

According to Figure 3.34, no emission signal of rhodamine B can be collected on the detector when the incident light was sent with 0° and 15° angle to the normal of the surface. If the incident light was sent to surface with 45° , there was signal, which did not look like an emission signal because the signal (purple line) might be due to reflection of the incident light beside the emission of Rhodamine B. A regular emission signal was obtained when the incident light came with either 30° or 60° . Since intensity of emission peak was slightly higher and maximum intensity was at expected wavelength (579 nm) for 30° , the angle of incident light was set as 30° and used in the rest of surface enhanced fluorescence measurements.

After optimization of incident light angle, experiments were done to observe the effect of distance between fluorophores to metal nanoparticles, types of distance layer (spacer).

3.7.3.1 Distance Optimization

Silica layer with different thickness were deposited on silver nanoparticles coated substrate by sputtering method. The sandwich type sample geometry (section 2.5) was used. 10 μl of 10^{-4} M fluorophore solution was dropped on bare glass slide. Silica deposited silver nanoparticles coated glass slide was placed on it and these two slides were clamped.

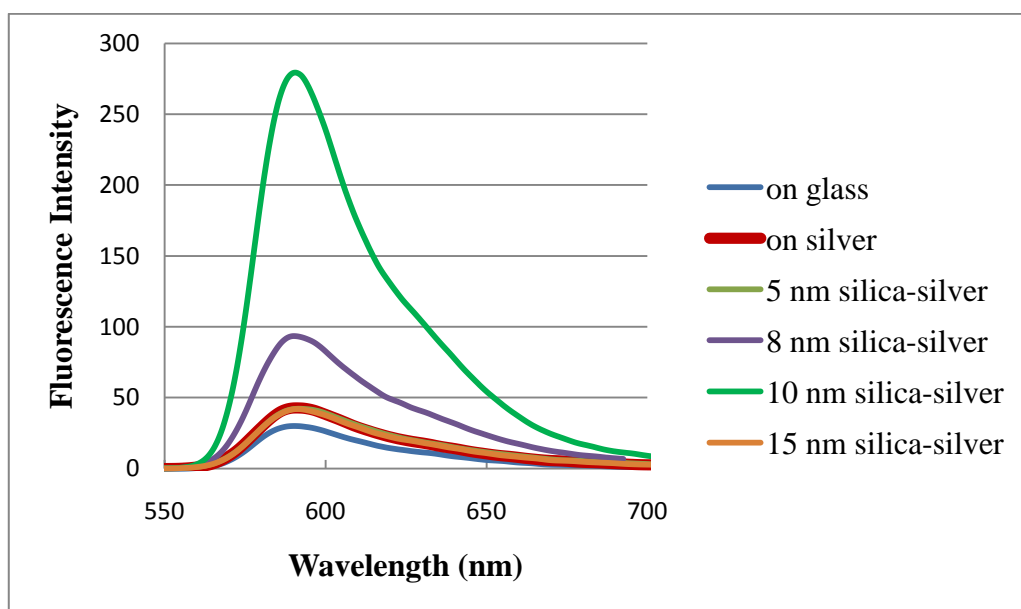


Figure 3.35 Distance optimization by silica layer between silver nanoparticles and rhodamine B molecules.

According to Figure 3.35, the emission signal intensity increased slightly when the rhodamine B molecules were in interaction with silver nanoparticles (red line). If a 5 nm distance provided by silica layer, the emission intensity slightly changed. When the thickness of silica layer was 8 nm, the enhancement could clearly be seen (purple line). 10 nm distance gave the maximum enhancement of fluorescence. However, when the distance increased 15 nm, the enhancement decreased.

In Table 3.4 the numeric values of emission intensity at maximum, enhancement factor were given.

Table 3.4 Silica thickness and obtained enhancement factors.

Relative Intensity	SEF Substrate	Enhancement Factor
25.0	Glass	1.00
42.5	Silver	1.70
41.8	5 nm silica-silver	1.67
92.8	8 nm silica-silver	3.70
280.0	10 nm silica-silver	11.2
41.7	15 nm silica-silver	1.67

According to Table 3.4, the best enhancement factor was calculated as 11.2 in which silica distance layer with 10 nm thickness was used.

Addition to rhodamine B, fluorescein was used to observe the distance effect (Figure 3.36) and distance of 10 nm was found for the best enhancement.

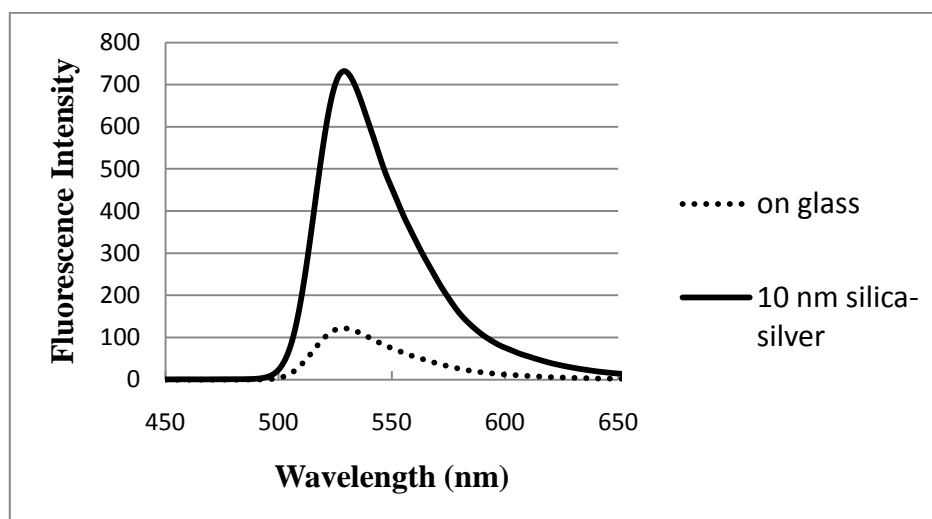


Figure 3.36 Enhanced fluorescence of fluorescein.

In Figure 3.36, enhancement factor was calculated as 6.03 for fluorescein solution. The enhancement factor obtained for fluorescein (6.03) was less than rhodamine B (11.2). This can be explained by comparing their quantum yield. The quantum yield

of rhodamine B is 0.70 whereas it is 0.95 for fluorescein. Therefore, fluorescence of rhodamine B was increased more than fluorescein.

3.7.3.2 Evaluation of Different Materials as a Spacer

After, distance between silver nanoparticle and fluorophores was optimized as 10 nm, different types of material (gold, zinc oxide, silica) were compared.

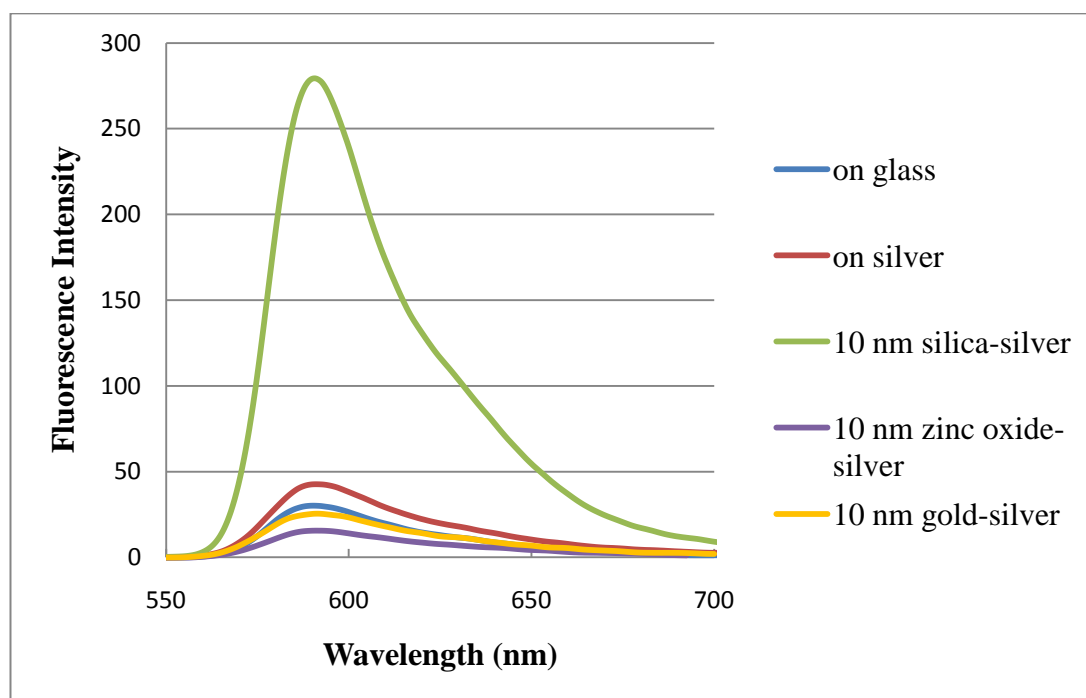


Figure 3.37 Effect of different spacer materials (10 nm thickness) to the fluorescence signal of rhodamine B.

In Figure 3.37, using zinc oxide or gold distance layer with 10 nm thickness in SEF substrates quenched the emission signal of rhodamine B. On the other hand, silica layer increased the emission intensity more than 10-fold. Therefore, silica was the only material among them that can be used as a spacer for SEF substrates.

Besides the spacer materials shown in Figure 3.37, stearic acid (SA) was studied to observe if it can be used as a spacer.

SA layers were prepared as described in section 3.8.3. Stearic acid layers were formed on silver nanoparticles deposited glass slides.

The SEF measurements of rhodamine B were taken with different number of stearic acid (SA) layers formed.

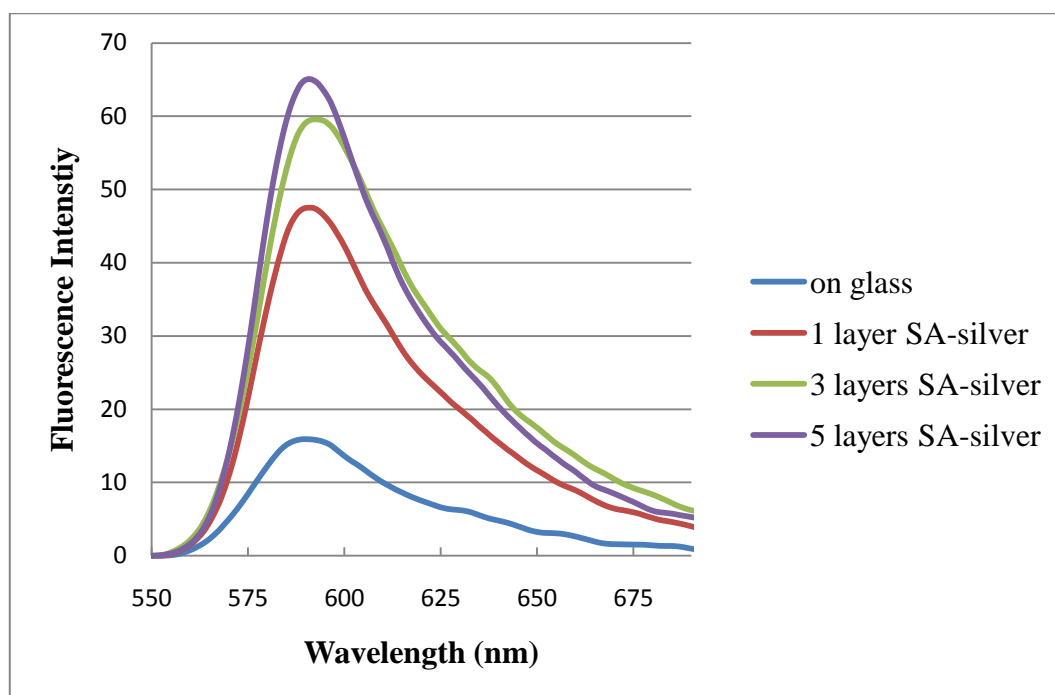


Figure 3.38 Effect of number of stearic acid (SA) layers the enhanced fluorescence of 5×10^{-5} M Rhodamine B solution.

As seen in Figure 3.38, stearic acid layers can act as a distance layer between fluorophores and silver nanoparticles. In literature, each stearic acid layer has a thickness of around 2.5 nm.

According to results in Figure 3.38, enhancement factor was calculated and tabulated in Table 3.5.

Table 3.5 Enhancement Factors with varying number stearic acid layers in SEF substrates.

Relative Intensity	Assembly	Theoretical distance (F-NPs)	Enhancement Factor
15.5	Glass	NA	1.0
-	Silver	NA	1.67
46	1 SA layer-silver	2.5 nm	3.0
57	3 SA layers-silver	7.5 nm	3.6
64	5 SA layers-silver	12.5 nm	4.3

The stearic acid layers provided an enhancement of rhodamine B fluorescence intensity, however not as strong as 10 nm silica layer provided.

CONCLUSION

In this study, silver and gold nanoparticles were prepared via chemical reduction method. In this method, amount of citrate was optimized in order to get the intense plasmon absorption and monodisperse silver colloid. Prepared silver particles had maximum plasmon absorption at 420 nm and arithmetic average diameter was 61.0 ± 11.2 nm. Prepared gold nanoparticles exhibited maximum plasmon absorption at 530 nm with 37.4 ± 2.3 nm arithmetic average diameter.

In addition, silica coated silver nanoparticles were prepared in our laboratory by sol-gel method. The plasmon absorption was shifted to the longer wavelength. By FE-SEM micrograph the thickness of silica coating was calculated as 43.2 ± 7.3 nm. Prior to deposition of prepared nanoparticles on the surface, glass slides were cleaned and modified. The derivatization of glass slide was done by immersion of the slide into aqueous APTES aqueous solution. Modified glass slides were immersed into colloid mixtures for the deposition of nanoparticles. Deposition immersion time was optimized by means of FE-SEM images and SERS measurements. Metal nanoparticle coated glass slide were stored at dark inside dessicator and purge with N_2 for 5 minutes after the lid was closed. Under these storage conditions, prepared substrates could preserve its properties for at least two weeks.

SERS spectroscopy was used not only to investigate the plasmon effect but also monitor the stability of nanoparticles coated substrates.

For surface enhanced fluorescence studies, different types of materials were used as a spacer between nanoparticle and fluorophore. Silica, zinc oxide and gold were deposited by physical vapor deposition techniques. Stearic acid layer was deposited by Langmuir-Blodgett system.

For solution based SEF studies, the emission intensity of fluorophores (rhodamine B and fluorescein) were quenched in the presence of silver and gold nanoparticles in the solution.

In surface studies, the best enhancement was observed when there was 10 nm silica as a spacer layer between nanoparticles and fluorophores. The enhancement factor was found as 11.2. When stearic acid was used as a spacer, significant enhancement was observed. The maximum enhancement factor was calculated as 4.3 when 5 layers of stearic acid were deposited on silver nanoparticles coated substrates.

Obtained enhancement factors show that, the enhancing ability of prepared SEF substrates have the potential to improve the sensitivity of fluorescence techniques utilized in many fields as long as an optimal distance is provided between fluorophores and metal nanoparticle and morphology of the metal nanoparticle is tuned for the fluorophore.

REFERENCES

- [1] Launouis H.,: *Applied Surface Science*, **2000**, 164
- [2] <http://www.scl.ameslab.gov/ABC/Articles/First-computer.html>, 2010.06.25
- [3] <http://ei.cs.vt.edu/~history/ENIAC.Richey.html>, 2010.06.27
- [4] Köhler M., Fritzsche W.,. *Nanotechnology:An Introduction to Nanostructuring Techniques*, **2007**, 1-2
- [5] Pitkethly M. J.,. *Nanomaterials -the driving force*. **2004**
- [6] <http://www.foresight.org/nano/history.html>, 2010.06.30
- [7] Sepeur S., *Nanotechnology: Technical Basics and Application*,, **2008**, 12-13
- [8] Karkare M., *Nanotechnology Fundamentals and Applications*, **2008**, 15-16
- [9] http://en.wikipedia.org/wiki/List_of_nanotechnology_applications, 2010.07.02
- [10] Vollath D., *Nanomaterials An Intoduction to Synthesis*, **2008**, 5-6
- [11] Barber I.C., and Freestone D.J., *Archaeometry*, **1990**, 32, 33-34
- [12] Freestone I, Meeks N., Sax M., Higgitt C, *Gold Bulletin*, **2007**, 40, 270
- [13] Raether H., *Surface Plasmons*, **1988**
- [14] Shalaev V.M., Kawara S., *Nanophotonics with Surface Plasmons*, **2007**, 143
- [15] Gray S. K., *Plasmonics* , **2007**, 2, 143-146

- [16] Lance K. K., Cronado E., Zhao L. L., Schatz G. C., *The Journal of Physical Chemistry B*, **2003**, 107, 668-677
- [17] Liz Marzan L. M., *Materials Today*, , **2004**, 26-31
- [18] Fleischmann M., Hendra P.J, McQuillan A. J., *Chemical Physics Letters*, **1974**, 26, 163
- [19] Jeanmarie D. L., Van Duyne R. P, *Journal of Electroanalytical Chemistry*, **1977**, 84, 1-20
- [20] Creighton J. A., Albrecht M. G., *Journal of American Chemical Society*, **1977**, 99, 5215
- [21] Lombardi J. R., *The Journal of Chemical Physics* , **1986**, 84, 4174-4180
- [22] Barbieri B., *A Short History of Fluorescence*
- [23] Drexhage K. H., Wolfe E., *Progress in Optics*, **1974**, 161-323
- [24] Aslan K., Grycznski I., Malicka J., Matveeva E., Lakowicz J. R., Geddes C. D., *Current Opinion in Biotechnology*, **2005**, 16, 55-62
- [25] Mayer C., Shalkhammer Th., **2005**, 8, 135-195
- [26] Fort E., Gresillon S., *Journal of Physics D:*, **2007**, 31
- [27] Mayer C., Stich N., Schalkhammer T. G. M., *Advances in Fluorescence Sensing Technology*, **2001**, 5, 37-46
- [28] Gersten J., Nitzan A., *Journal of Chemical Physics*, **1981**, 75, 1139-1152
- [29] Skoog D. A., West D. M., Holler F. J. *Fundamentals of Analytical Chemistry*, **1996**, 7, 603
- [30] Strickler S. J., Berg R. A., **1962**, 37, 814-822

- [31] Skoog A. D., Holler J. F., Nieman T. A., *Principles of Instrumental Analysis*, **1998**, 5, 361
- [32] Lakowicz J. R., *Principles of Fluorescence Spectroscopy*, **2006**, 11-15
- [33] Geddes D. C., Grczynski I, Malicka J., Gryczynski Z., Lakowicz J. R., *Combinational Chemistry and High Throughput Screening*, **2003**, 6, 109-117
- [34] Thompson R. B., *Fluorescence Sensors and Biosensors*, **2006**, 121-181
- [35] Kruszewski S., Wybranonwski T., Cyrankiewicz M., Ziomkowska B., Pawlaczyk A., *Acta Physica Polonica A*, **2008**, 113, 1599-1608
- [36] Lakowicz J. R., *Analytical Biochemistry*, **2001**, 298, 1-24
- [37] Campion A., Gallio A. R., Harris C. B., Robota H. J., Whitmore P. M., *Chemical Physics Letters*, **1980**, 73, 447-450
- [38] Shik Chi Y., Ryung Byon H., Lee B. S., Kong. B., Choi C. H., Choi S. I., **2008**, 18, 3395-3402
- [39] Yun C. S., Javier A., Jennings T., Fisher M., Hira S., Peterson S., Hopkins B., Reich N. O., Strouse G. F., *Journal of American Chemical Society*, **2005**, 127, 3115-3119
- [40] Zhang J., Lakowicz J. R., *Optics Express*, **2007**, 15, 2598-2606
- [41] Aslan K., Previte Micheal J. R., Zhang Y., Geddes C. D., *Journal of Physical Chemistry*, **2008**, 112, 18368-18375
- [42] Fu Y., Lakowicz J. R., *Journal of Physical Chemistry*, **2006**, 110, 22557-22562
- [43] Jennings T. L., Singh M. P., Strouse G. F., *Journal of American Chemical Society*, **2006**, 128, 5462-5467
- [44] Ray K., Badagu R., Lakowicz J. R., *Langmuir*, **2006**, 22, 8374-8378

- [45] Lakowicz J. R., Geddes C. D., *Fluorescence Sensing*, PCT/US2003/013411
2003
- [46] Lukomkska J., Joanna M., Grycznski I., Lakowicz J. R., *Journal of Fluorescence*, **2004**, 14, 417-423
- [47] Tam F., Goodrich P. G., Johnson B. R., Hales N. J., *Nano Letters*, **2007**, 7, 496-501
- [48] Xie F., Baker M. S., Goldys M. E., **2008**, 20, 1788-1797
- [49] Aslan K., Leonenko Z., Lakowicz J. R., Geddes C. D., *Journal of Physical Chemistry*, **2005**, 109, 3157-3162
- [50] Geddes C. D., Cao H., Gryczynski I., Gryczynski Z., Fang J., Lakowicz J. R., *Journal of Physical Chemistry*, **2003**, 107, 3443-3449
- [51] Yan F., Wabuyele M. B., Griffin G. D., Vo-Dinh T., *Plasmonics in Biology and Medicine*, **2004**
- [52] dos Santos D. S., Aroca, F. R, *The Analyst*, **2007**, 132, 450-454
- [53] Goulet J. G. P., dos Santos D., Alvares-Puebla A. R., Oliveira O. N., Aroca R. F., *Langmuir*, **2005**, 21, 5576-5581
- [54] Zhang Y., Padhyay A., Sevillaja J. E., Guerrant R. L., Geddes C. D., *Journal of Physical Chemistry*, **2010**, 114, 7575-7581
- [55] Zhang Y., Dragan A., Geddes C. D., *Journal of Physical Chemistry*, **2009**, 113, 15881-15816
- [56] Soğancı İ. M., Nizamoğlu S., Mutlugun E, Akın O., Demir H. V., *Optics Express*, **2007**, 15, 14289-14298
- [57] Mangeat T., Berthier A., Elie-Caille C., Perrin M., Boireau W., Pieralli and Wacogne B., *Laser Physics*, **2009** , 19, 252-258

- [58] Krishanu R., Badugu R., and Lakowicz J. R., *Journal of Physical Chemistry C Nanomater Interfaces*, **2007**, 111, 7091-7097
- [59] Stranik O., McEvoy H. M., McDonagh C., MacCraith B. D., *Sensors and Actuators B*, **2005**, 107, 148-153
- [60] Leveque-Fort S., Fort E., Le Moal E., Lacharme J., Fontaine-Aupart M., Ricolleau C., *Plasmonics in Biology and Medicine*, **2004**, 5327, 29-36
- [61] DeSaja-Gonzalez J., Aroca R., Nagao Y., DeSaja J. A., *Spectrochimica Acta Part A*, **1997**, 53, 173-181
- [62] Ondrej Stranik, Robert Nooney, Colette McDonagh, and Brian D. MacCraith, *Nanocrystals, Nanoparticles, and Quantum Dots II*, **2005**, 5824, 79-85
- [63] Aslan K., Leonenko Z., Lakowicz J. R. Geddes C. D., *Journal of Fluorescence*, **2005**, 15, 643-654
- [64] Ianoul A., Bergeron A., *Langmuir*, **2006**, 22, 10217-10222
- [65] Tovmachenko O. G., Graf C., vanden Heuvel J., van Blaaderen A., Gerritsen H., *Advanced Materials*, **2006**, 18, 91-95
- [66] Zhang Y., Aslan K., Previte J.R., *Applied Physics Letters*, **2007**, 90, 173116
- [67] Mattox M. D., *Handbook of Physical Vapor Deposition (PVD) Processing* **1998**, 22-24
- [68] Harsha S. K., *Principles of Physical Vapor Deposition of Thin Films*, **2006**
- [69] <http://www.siliconfareast.com/sputtering.html>, 2010.07.20
- [70] Nunez. M., *Progress in Electrochemistry Research*, **2005**, 67
- [71] Petty C. M., *Langmuir-Blodgett Films: an Introduction*, **1996**, 39

- [72] <http://www.horiba.com/scientific/products/raman-spectroscopy/raman-systems/research-raman/details/labram-hr-130>, 2010.07.25
- [73] <http://www.vaksis.com/urun.php?ID=1024>, 2010.07.25
- [74] www.ksvltd.com/content/index/minitrough, 2010.07.25
- [75] Lee P. C., Meisel D., *Journal of Physical Chemistry*, **1982**, 86, 3391-3395
- [76] Stöber W., Fink aA., Bohn E., *Journal of Colloid and Interface Science*, **1968**, 26, 62-69
- [77] Lv Y., Liu H., Wang Z., Hao L., Liu J., Wang Y., Du G., Zhan J., Wang J., *Polymers for Advanced Technologies*, **2008**, 19, 1455-1460
- [78] *Journal of Chemical Physics*, 116, 6755-6759
- [79] Mock J., Barbic M., Smith D.R., Schultz D.A., Schultz S., *Journal of Chemical Physics*, **2002**, 116, 6755-6759
- [80] Aslan K., Wu M., Lakowicz J. R., Geddes C. D., **2006**, 129. 1524-1525
- [81] Sancı R., Volkan M., *Chemical Sensors and Actuators B*: **2009**, 139, 150-155.
- [82] Sokolov K., Chumanov G., Cotton M. T., *Journal of Analytical Chemistry*, **1998**, 70, 3898-3905
- [83] Stiles P.L., Dieringer J. A., Shah N. C., Van Duyne P. R., *Annual Reviews of Analytical Chemistry*, **2008**, 1, 601-625